PHYSICAL REVIEW D **68**, 084010 (2003)

Exact general relativistic perfect fluid disks with halos

Daniel Vogt*
Instituto de Física Gleb Wataghin, Universidade Estadual de Campinas 13083-970 Campinas, São Paulo, Brazil

Patricio S. Letelier†
Departamento de Matemática Aplicada-IMECC, Universidade Estadual de Campinas, 13081-970 Campinas, São Paulo, Brazil

(Received 26 June 2003; revised manuscript received 4 August 2003; published 24 October 2003)

Using the well-known ''displace, cut, and reflect'' method used to generate disks from given solutions of Einstein's field equations, we construct static disks made of a perfect fluid based on vacuum Schwarzschild's solution in isotropic coordinates. The same method is applied to different exact solutions to Einstein's equations that represent static spheres of perfect fluids. We construct several models of disks with axially symmetric perfect fluid halos. All disks have some common features: surface energy density and pressure decrease monotonically and rapidly with the radius. As the ''cut'' parameter a decreases, the disks become more relativistic, with the surface energy density and pressure more concentrated near the center. Also, regions of unstable circular orbits are more likely to appear for high relativistic disks. Parameters can be chosen so that the sound velocity in the fluid and the tangential velocity of test particles in circular motion are less than the velocity of light. This tangential velocity first increases with radius and reaches a maximum.

DOI: 10.1103/PhysRevD.68.084010 PACS number(s): 04.20.Jb, 04.40.−b, 97.10.Gz

I. INTRODUCTION

Axially symmetric solutions of Einstein's field equations corresponding to disklike configurations of matter are of great astrophysical interest, since they can be used as models of galaxies or accretion disks. These solutions can be static or stationary and with or without radial pressure. Solutions for static disks without radial pressure were first studied by Bonnor and Sackfield [1], and Morgan and Morgan [2], and with radial pressure by Morgan and Morgan [3]. Disks with radial tension have been considered in [4], and models of disks with electric fields [5], magnetic fields [6], and both magnetic and electric fields have been introduced recently [7]. Solutions for self-similar static disks were analyzed by Lynden-Bell and Pineault [8] and Lemos [9]. The superposition of static disks with black holes were considered by Lemos and Letelier [10–12] and Klein [13]. Also Bičák, Lynden-Bell, and Katz [14] studied static disks as sources of known vacuum spacetimes and Bičák, Lynden-Bell, and Pichon [15] found an infinite number of new static solutions. For a recent survey on relativistic gravitating disks, see [16].

The principal method to generate the above mentioned solution is the ''displace, cut and reflect'' method. One of the main problems with the solutions generated by using this simple method is that usually the matter content of the disk is anisotropic; i.e., the radial pressure is different from the azimuthal pressure. In most of the solutions the radial pressure is null. This made these solutions rather unphysical. Even though, one can argue that when no radial pressure is present stability can be achieved if we have two circular streams of particles moving in opposite directions (the counterrotating hypothesis, see for instance [14]).

In this article we apply the displace, cut, and reflect method to spherically symmetric solutions of Einstein's field equations in isotropic coordinates to generate static disks made of a *perfect fluid*, i.e., with radial pressure equal to tangential pressure and also disks of perfect fluid surrounded by a halo made of perfect fluid matter.

The article is organized as follows. Section II gives an overview of the displace, cut, and reflect method. Also we present the basic equations used to calculate the main physical variables of the disks. In Sec. III we apply the formalism to obtain the simplest model of the disk, which is based on Schwarzschild's vacuum solution in isotropic coordinate. The generated class of disks is made of a perfect fluid with well behaved density and pressure. Section IV presents some models of disks with halos obtained from different known exact solutions of Einstein's field equations for static spheres of perfect fluid in isotropic coordinates. In Sec. V we give some examples of disks with halo generated from spheres composed of fluid layers. Section VI is devoted to discussion of the results.

II. EINSTEIN EQUATIONS AND DISKS

For a static, spherically symmetric spacetime the general line element in isotropic spherical coordinates can be cast as

$$ds^2 = e^{\nu(r)}dt^2 - e^{\lambda(r)}[dr^2 + r^2(d\theta^2 + \sin^2\theta d\varphi^2)]. \quad (1)$$

In cylindrical coordinates (t,R,z,φ) the line element (1) takes the form

$$ds^2 = e^{\nu(R,z)}dt^2 - e^{\lambda(R,z)}(dR^2 + dz^2 + R^2 d\varphi^2). \quad (2)$$

The metric of the disk will be constructed using the well known displace, cut, and reflect method that was used by Kuzmin [17] in Newtonian gravity and later in general relativity by many authors [4–16]. The material content of the disk will be described by functions that are distributions with support on the disk. The method can be divided in the following steps that are illustrated in Fig. 1. First, in a space

*Email address: danielvt@ifi.unicamp.br
†Email address: letelier@ime.unicamp.br

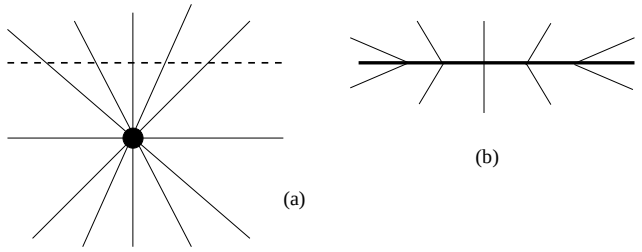

FIG. 1. An illustration of the displace, cut, and reflect method for the generation of disks. In (a) the spacetime with a singularity is displaced and cut by a plane (dotted line); in (b) the part with singularities is disregarded and the upper part is reflected on the plane.

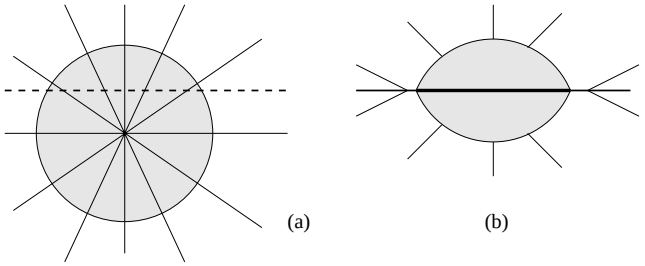

FIG. 2. An illustration of the displace, cut, and reflect method for the generation of disks with halos. In A the sphere of perfect fluid is displaced and cut by a plane (dotted line); in (b) the lower part is disregarded and the upper part is reflected on the plane.

wherein we have a compact source of gravitational field, we choose a surface (in our case, the plane $z=0$) that divides the space in two pieces: one with no singularities or sources and the other with the sources. Then we disregard the part of the space with singularities and use the surface to make an inversion of the nonsingular part of the space. This results in a space with a singularity that is a delta function with support on $z=0$. This procedure is mathematically equivalent to make the transformation $z\rightarrow|z|+a$, with a as constant. In the Einstein tensor we have first and second derivatives of z. Since $\partial_z|z|=2\vartheta(z)-1$ and $\partial_{zz}|z|=2\delta(z)$, where $\vartheta(z)$ and $\delta(z)$ are, respectively, the Heaviside function and the Dirac distribution. Therefore the Einstein field equations will separate in two different pieces [18]: one valid for $z\neq0$ (usual Einstein's equations) and the other involving distributions with an associated energy-momentum tensor $T_{ab}=Q_{ab}\delta(z)$ with support on $z=0$. For metric (2), the nonzero components of Q_{ab} are

$$Q_t^t=\frac{1}{16\pi}[-b^{zz}+g^{zz}(b_R^R+b_z^z+b_\varphi^\varphi)], \tag{3}$$

$$Q_R^R=Q_\varphi^\varphi=\frac{1}{16\pi}[-b^{zz}+g^{zz}(b_t^t+b_R^R+b_z^z)], \tag{4}$$

where b_{ab} denotes the jump of the first derivatives of the metric tensor on the plane $z=0$,

$$b_{ab}=g_{ab,z}|_{z=0^+}-g_{ab,z}|_{z=0^-}, \tag{5}$$

and the other quantities are evaluated at $z=0^+$. The "true" surface energy-momentum tensor of the disk can be written as $S_{ab}=\sqrt{-g_{zz}}Q_{ab}$, thus the surface energy density σ and the radial and azimuthal pressures or tensions (P) read

$$\sigma=\sqrt{-g_{zz}}Q_t^t, \quad P=-\sqrt{-g_{zz}}Q_R^R=-\sqrt{-g_{zz}}Q_\varphi^\varphi. \tag{6}$$

Note that when the same procedure is applied to an axially symmetric spacetime in Weyl coordinates we have $Q_R^R=0$, i.e., we have no radial pressure or tension.

This procedure in principle can be applied to any spacetime solution of the Einstein equations with or without source (stress tensor). The application to a static sphere of perfect fluid is schematized in Fig. 2. The sphere is displaced and cut by a distance a less than its radius r_b. The part of the space that contains the center of the sphere is disregarded. After the inversion of the remaining space, we end up with a disk surrounded by a cap of perfect fluid. The properties of the inner part of the disk will depend on the internal fluid solution, but if the internal spherical fluid solution is joined to the standard external Schwarzschild solution, the physical properties of the outer part of the disk will be those originated from Schwarzschild's vacuum solution.

In isotropic coordinates the matching at the boundary of the fluid sphere leads to four continuity conditions: metric functions e^λ and e^ν together with their first derivatives with respect to the radial coordinate should be continuous across the boundary. In addition, to have a compact body the pressure at the surface of the material sphere has to drop to zero. Also to have a meaningful solution the velocity of sound, $V^2=dp/d\rho$, should be restricted to the interval $0\leqslant V<1$.

The Einstein equations for a static, spherically symmetric spacetime in isotropic coordinates for a perfect fluid source give us that density ρ and pressure p are related to the metric functions by

$$\rho=-\frac{e^{-\lambda}}{8\pi}\left[\lambda''+\frac{1}{4}(\lambda')^2+\frac{2\lambda'}{r}\right], \tag{7}$$

$$p=\frac{e^{-\lambda}}{8\pi}\left[\frac{1}{4}(\lambda')^2+\frac{1}{2}\lambda'\nu'+\frac{1}{r}(\lambda'+\nu')\right], \tag{8}$$

where primes indicate differentiation with respect to r.

Also static spheres composed of various layers of fluid can be used to generate disks with halos of fluid layers (see Fig. 3). The disk will then be composed of different axial symmetric "pieces" glued together. The matching conditions at the boundary of adjacent spherical fluid layers in isotropic coordinates involves four continuity conditions: the two metric functions e^λ and e^ν, the first derivative of λ with respect to the radial coordinate, and the pressure should be continuous across the boundary. At the most external boundary, the metric functions e^λ and e^ν and their first derivatives with respect to the radial coordinate should be continuous across the boundary; also the pressure there should go to zero.

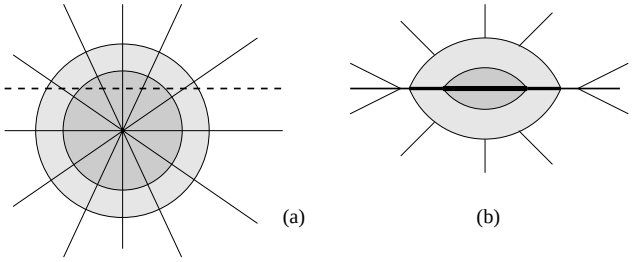

FIG. 3. An illustration of the displace, cut, and reflect method for the generation of disks with various layers of halos. In (a) the sphere with different layers of fluid is displaced and cut with a plane (dotted line); in (b) the field is reflected on the plane.

III. THE SIMPLEST DISK

We first apply the displace, cut, and reflect method to generate disks discussed in the previous section and depicted in Fig. 1 to the Schwarzschild metric in isotropic coordinates (t,r,θ,φ),

$$ds^2=\frac{\left(1-\frac{m}{2r}\right)^2}{\left(1+\frac{m}{2r}\right)^2}dt^2-\left(1+\frac{m}{2r}\right)^4 \times[dr^2+r^2(d\theta^2+\sin^2\theta d\varphi^2)]. \tag{9}$$

Expressing solution (9) in cylindrical coordinates, and using Eqs. (3)–(6), we obtain a disk with surface energy density σ and radial and azimuthal pressures (or tensions) P given by

$$\sigma=\frac{4ma}{\pi(m+2\sqrt{R^2+a^2})^3}, \tag{10}$$

$$P=-\frac{2m^2a}{\pi(m+2\sqrt{R^2+a^2})^3(m-2\sqrt{R^2+a^2})}. \tag{11}$$

The total mass of the disk can be calculated with the help of Eq. (10):

$$\mathcal{M}=\int_0^\infty\int_0^{2\pi}\sigma\sqrt{g_{RR}g_{\varphi\varphi}}dRd\varphi=\frac{m}{4a}(m+4a). \tag{12}$$

Equation (10) shows that the disk's surface energy density is always positive (weak energy condition). Positive values (pressure) for the stresses in azimuthal and radial directions are obtained if $m<2\sqrt{R^2+a^2}$. The strong energy condition $\sigma+P_{\varphi\varphi}+P_{RR}=\sigma+2P>0$ is then satisfied. These properties characterize a fluid made of matter with the usual gravitational attractive property. This is not a trivial property of these disks since it is known that the displace, cut, and reflect method sometimes gives disks made of exotic matter such as cosmic strings, see for instance [19].

Another useful parameter is the velocity of sound propagation, V, defined as $V^2=dP/d\sigma$, which can be calculated using Eqs. (10) and (11):

$$V^2=\frac{m(4\sqrt{R^2+a^2}-m)}{3(m-2\sqrt{R^2+a^2})^2}. \tag{13}$$

The condition $V^2<1$ (no tachyonic matter) imposes the inequalities $m<\sqrt{R^2+a^2}$ or $m>3\sqrt{R^2+a^2}$. If the pressure condition and the speed of sound less than the speed of light condition are to be simultaneously satisfied, then $m<\sqrt{R^2+a^2}$. This inequality will be valid in all the disk if $m<a$.

With the presence of radial pressure one does not need the assumption of streams of rotating and counterrotating matter usually used to explain the stability of static disk models. However, a tangential velocity (rotation profile) can be calculated by assuming that a test particle moves in a circular geodesic on the disk. We tacitly assume that this particle only interacts gravitationally with the fluid. This assumption is valid for the case of a particle moving in a very diluted gas such as the gas made of stars that models a galaxy disk.

The geodesic equation for the R coordinate obtained from metric (2) is

$$e^\lambda\ddot{R}+\tfrac{1}{2}(e^\nu)_{,R}\dot{t}^2-\tfrac{1}{2}(e^\lambda)_{,R}(\dot{R}^2+\dot{z}^2)-\tfrac{1}{2}(e^\lambda R^2)_{,R}\dot{\varphi}^2=0. \tag{14}$$

For circular motion on the $z=0$ plane, $\dot{R}=\ddot{R}=0$ and $\dot{z}=0$, then Eq. (14) reduces to

$$\frac{\dot{\varphi}^2}{\dot{t}^2}=\frac{(e^\nu)_{,R}}{(e^\lambda R^2)_{,R}}. \tag{15}$$

The tangential velocity measured by an observer at infinity is then

$$v_c^2=-\frac{g_{\varphi\varphi}}{g_{tt}}\left(\frac{d\varphi}{dt}\right)^2=R^2\frac{e^\lambda(e^\nu)_{,R}}{e^\nu(R^2e^\lambda)_{,R}}. \tag{16}$$

From the metric on the disk,

$$e^\nu=\frac{\left(1-\frac{m}{2\sqrt{R^2+a^2}}\right)^2}{\left(1+\frac{m}{2\sqrt{R^2+a^2}}\right)^2} \text{ and } e^\lambda=\left(1+\frac{m}{2\sqrt{R^2+a^2}}\right)^4, \tag{17}$$

we find that Eq. (16) can be cast as

$$v_c^2=\frac{mR^2}{\left(1-\frac{m}{2\sqrt{R^2+a^2}}\right)\left[(R^2+a^2)^{3/2}+\frac{m}{2}(a^2-R^2)\right]}. \tag{18}$$

For $R\gg a$, Eq. (18) goes as $v_c=(m/R)^{1/2}$, the Newtonian circular velocity.

To determine the stability of circular orbits on the disk's plane, we use an extension of Rayleigh [20,21] criteria of stability of a fluid at rest in a gravitational field,

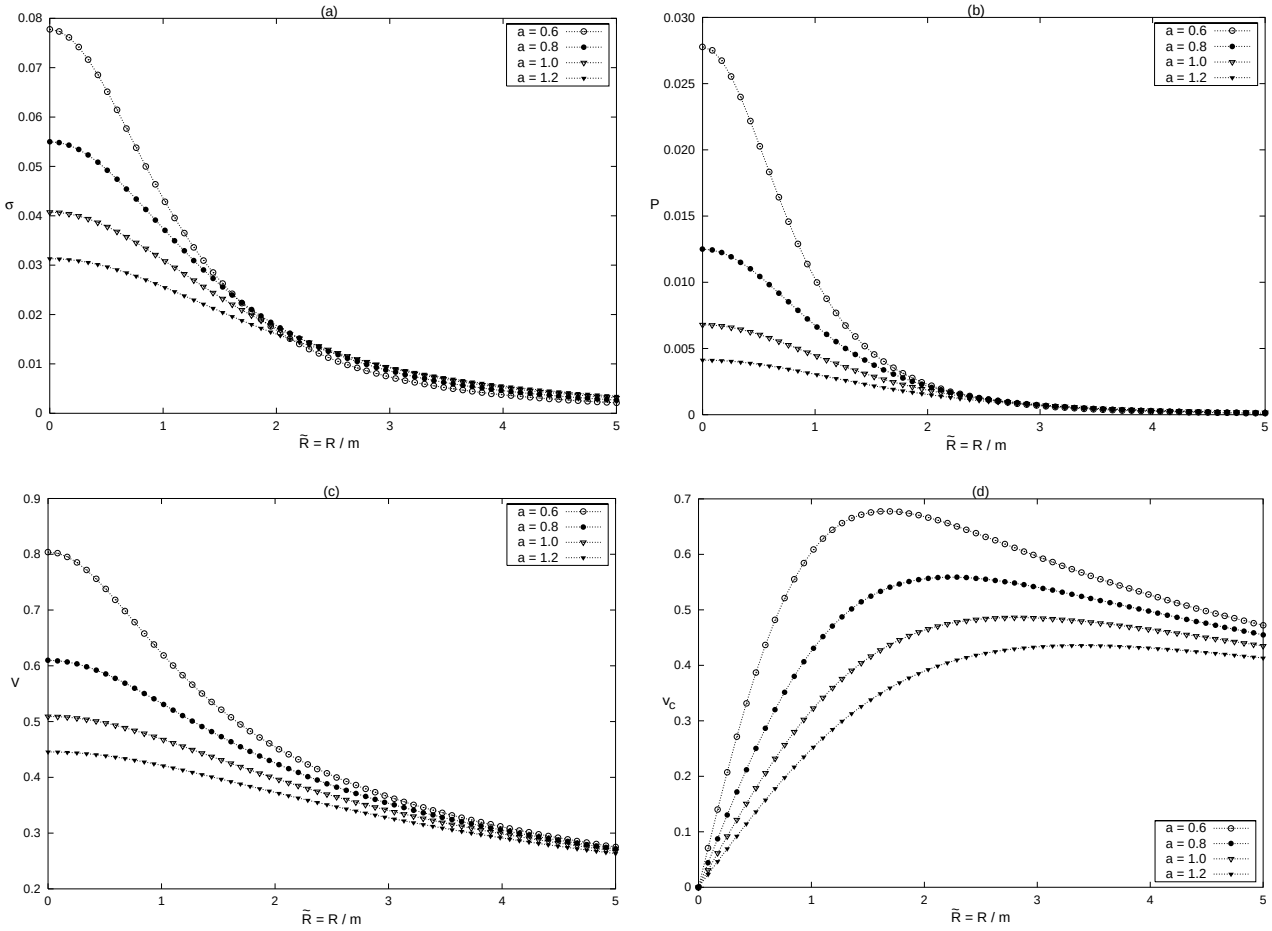

FIG. 4. (a) The surface energy density σ, (b) pressures P, (c) sound velocity V, and (d) tangential velocity v_c (rotation curve or rotation profile) with $m=0.5$ and $a=0.6,0.8,1.0$, and 1.2 as functions of $\tilde{R}=R/m$. We use geometric units $G=c=1$.

$$h\frac{dh}{dR}>0, \tag{19}$$

where h is the specific angular momentum of a particle on the disk's plane:

$$h=-g_{\varphi\varphi}\frac{d\varphi}{ds}=-g_{\varphi\varphi}\frac{d\varphi}{dt}\frac{dt}{ds}. \tag{20}$$

Using Eq. (15) and the relation

$$1=e^{\nu}\left(\frac{dt}{ds}\right)^2-R^2e^{\lambda}\left(\frac{d\varphi}{ds}\right)^2, \tag{21}$$

one obtains the following expression for h:

$$h=R^2e^{\lambda}\sqrt{\frac{(e^{\nu})_{,R}}{e^{\nu}(R^2e^{\lambda})_{,R}-R^2e^{\lambda}(e^{\nu})_{,R}}}. \tag{22}$$

For functions (17), Eq. (22) reads

$$h=\frac{2\sqrt{m}R^2\left(1+\dfrac{m}{2\sqrt{R^2+a^2}}\right)^2(R^2+a^2)^{1/4}}{\sqrt{4(R^2+a^2)^2-8mR^2\sqrt{R^2+a^2}+m^2(R^2-a^2)}}. \tag{23}$$

The stability criterion is always satisfied for $a/m\gtrsim 1.016$.

In Figs. 4(a)–4(d) we show, respectively, the surface energy density, pressures, the sound velocity, and curves of the tangential velocity (rotation curves) [Eq. (18)] with $m=0.5$ and $a=0.6,0.8,1.0$, and 1.2 as functions of $\tilde{R}=R/m$. Figures 5(a)–5(c) display, respectively, the surface energy density, pressures, and sound velocity with parameters $a=1.0$ and $m=0.2,0.4,0.6$, and 0.8 as as functions of $\tilde{R}=R/m$. We see that the first three quantities decrease monotonically with the radius of the disk, as can be checked from Eqs. (10), (11), and (13). Energy density decreases rapidly enough in principle, to, define a cut off radius and consider the disk as finite.

IV. DISKS WITH HALOS

Now we study some disks with halos constructed from several exact solutions of the Einstein equations for static

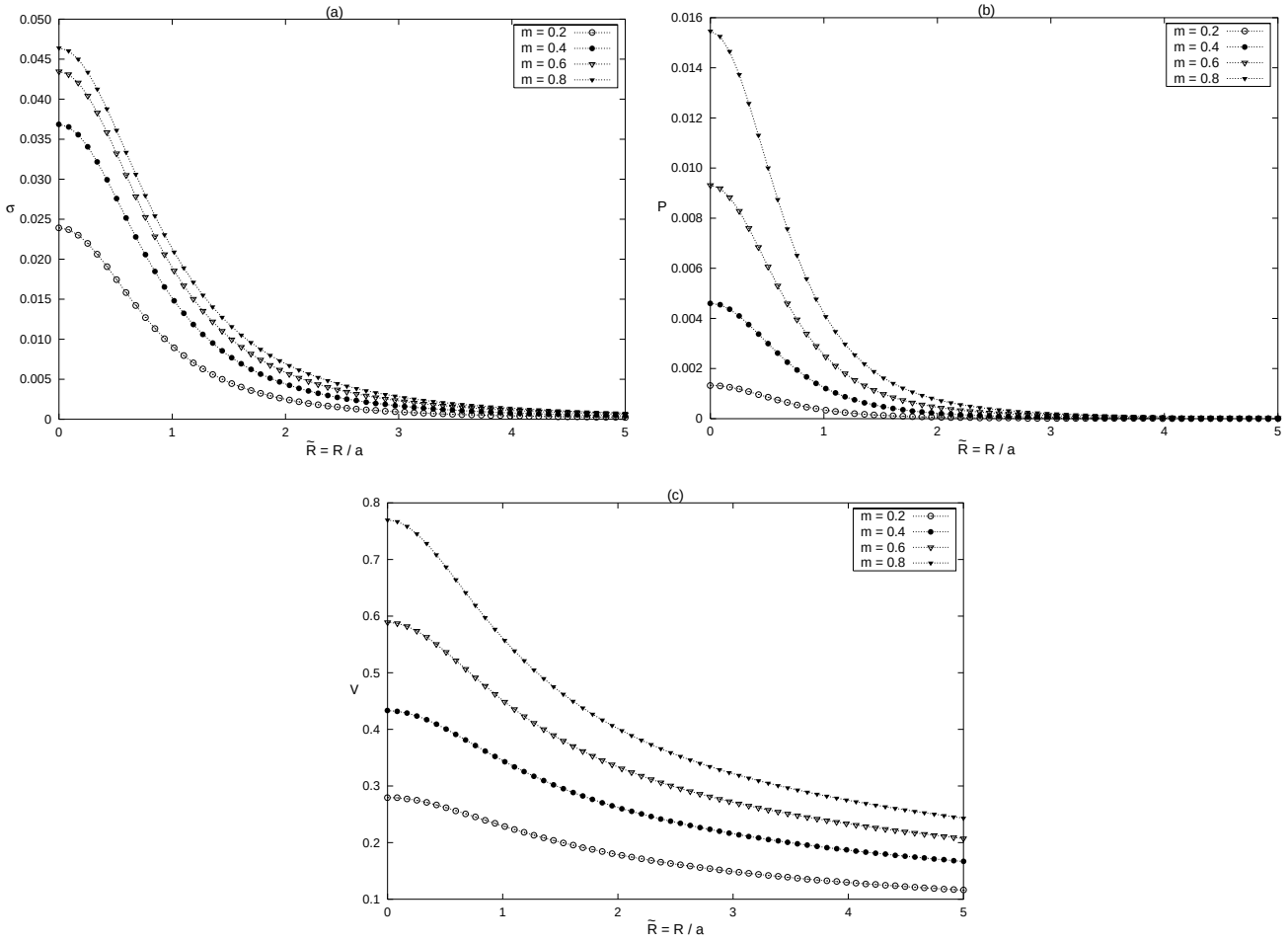

FIG. 5. (a) The surface energy density σ, (b) pressures P, and (c) sound velocity V with $a=1.0$ and $m=0.2,0.4,0.6,$ and 0.8 as functions of $\tilde{R}=R/a$.

spheres of perfect fluid. A survey of these classes of solutions is presented in [22].

A. Buchdahl's solution

The first situation that we shall study is similar to the one depicted in Fig. 2 wherein we start with a sphere of perfect fluid. This case will not be exactly the same as the one presented in the mentioned figure because the sphere has no boundary. Hence the generated disk will be completely immersed in the fluid. An example of exact solution of the Einstein equations that represent a fluid sphere with no boundary is the the Buchdahl solution that may be regarded as a reasonably close analog to the classical Lane-Emden index 5 polytrope [23]. The metric functions for this solution are:

$$e^{\nu}=\left(\frac{1-\frac{A}{\sqrt{1+kr^2}}}{1+\frac{A}{\sqrt{1+kr^2}}}\right)^2, \quad e^{\lambda}=\left(1+\frac{A}{\sqrt{1+kr^2}}\right)^4, \quad (24)$$

where A and k are constants. Far from the origin the solution goes over into the external Schwarzschild metric when $m=2A/\sqrt{k}$. The density, pressure, and sound velocity are given by

$$\rho=\frac{3Ak}{2\pi(A+\sqrt{1+kr^2})^5},$$

$$p=\frac{kA^2}{2\pi(-A+\sqrt{1+kr^2})(A+\sqrt{1+kr^2})^5}, \quad (25)$$

$$V^2=\frac{2A(-2A+3\sqrt{1+kr^2})}{15(A-\sqrt{1+kr^2})^2}. \quad (26)$$

The condition $V<1$ is satisfied for $A<[(18-\sqrt{39})/19]\sqrt{1+kr^2}$.

Using Eq. (24) and Eqs. (3)–(6), we get the following expressions for the energy density, pressure, and sound velocity of the disk:

$$\sigma=\frac{akA}{\pi[A+\sqrt{1+k(R^2+a^2)}]^3}, \quad (27)$$

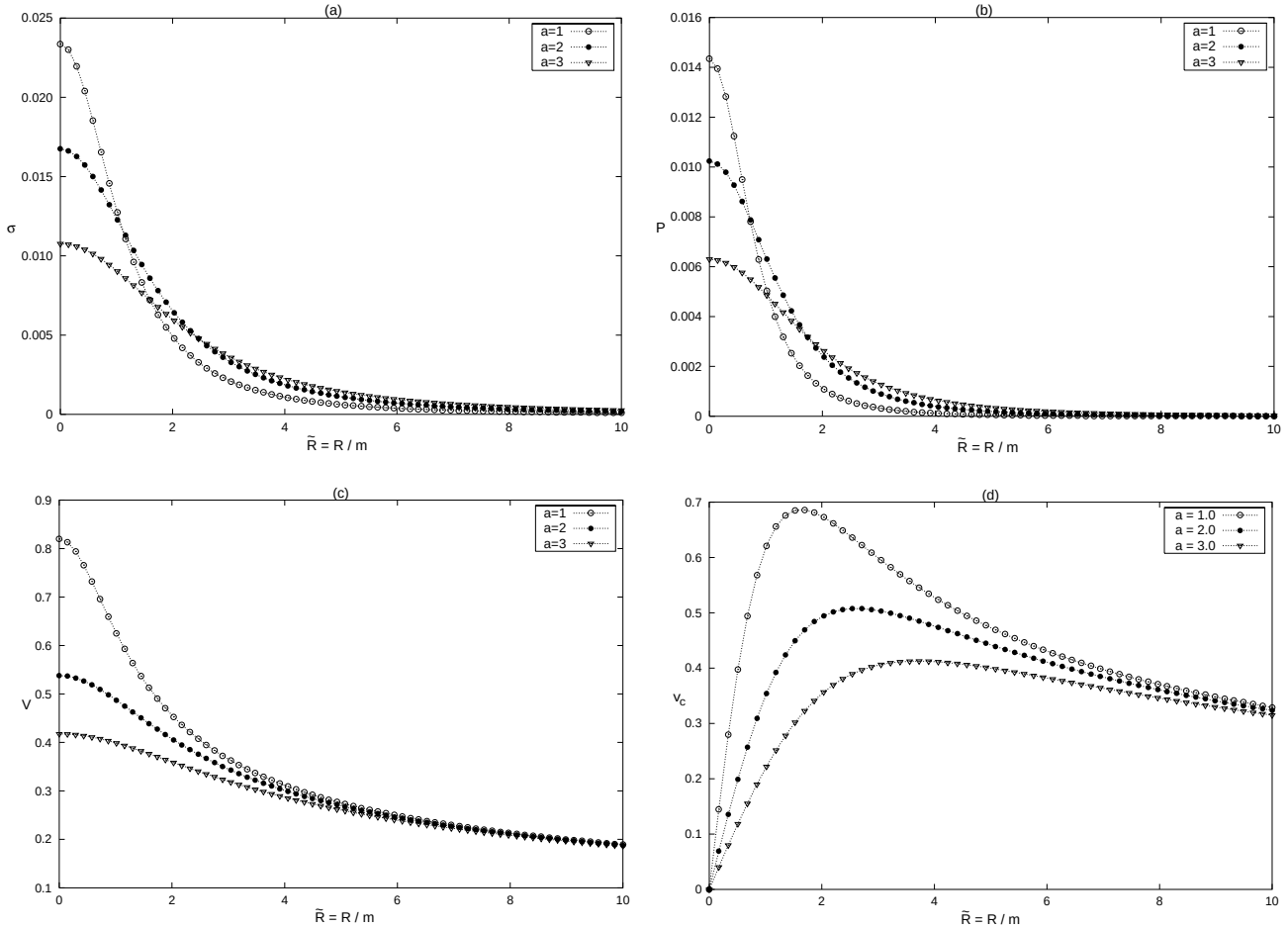

FIG. 6. (a) The surface energy density σ, Eq. (27), (b) the pressure P, Eq. (28), (c) the velocity of sound V, Eq. (29), and (d) the tangential velocity v_c, Eq. (30), for the disk with $A=0.6$ and $k=1$ for $a=1$, 2, and 3 as functions of $\tilde{R}=R/m$.

$$P=\frac{akA^2}{2\pi[-A+\sqrt{1+k(R^2+a^2)}][A+\sqrt{1+k(R^2+a^2)}]^3}, \tag{28}$$

$$V^2=\frac{A[-A+2\sqrt{1+k(R^2+a^2)}]}{3[A-\sqrt{1+k(R^2+a^2)}]^2}. \tag{29}$$

The conditions $V<1$ and $P>0$ are both satisfied if $A<\frac{1}{2}\sqrt{1+ka^2}$. Figures 6(a)–6(d) show, respectively, σ, P, V, and rotation curves, Eq. (30), as functions of $\tilde{R}=R/m$ for the disk calculated from Buchdahl's solution.

In Figs. 7(a) and 7(b) we show, respectively, the density ρ together with pressure p, and sound velocity V of the halo along the axis z for $A=0.6;k=1$ and $a=1$. Note that in this solution there is no boundary of the fluid sphere: the disk is completely immersed in the fluid.

The tangential velocity v_c calculated from metric coefficients (24) is

$$v_c^2=\frac{2AkR^2}{(1-A/\sqrt{1+k(R^2+a^2)})\{[1+k(R^2+a^2)]^{3/2}+A[1+k(a^2-R^2)]\}}. \tag{30}$$

For $R\gg a$, Eq. (30) goes as $v_c=(2A)^{1/2}/(R^{1/2}k^{1/4})$. The specific angular momentum follows from Eqs. (22) and (24):

$$h=\frac{\sqrt{2Ak}R^2\left(1+\dfrac{A}{\sqrt{1+k(R^2+a^2)}}\right)^2[1+k(R^2+a^2)]^{1/4}}{\sqrt{[1+k(R^2+a^2)]^2-4AkR^2\sqrt{1+k(R^2+a^2)}-A^2[1+k(a^2-R^2)]}}. \tag{31}$$

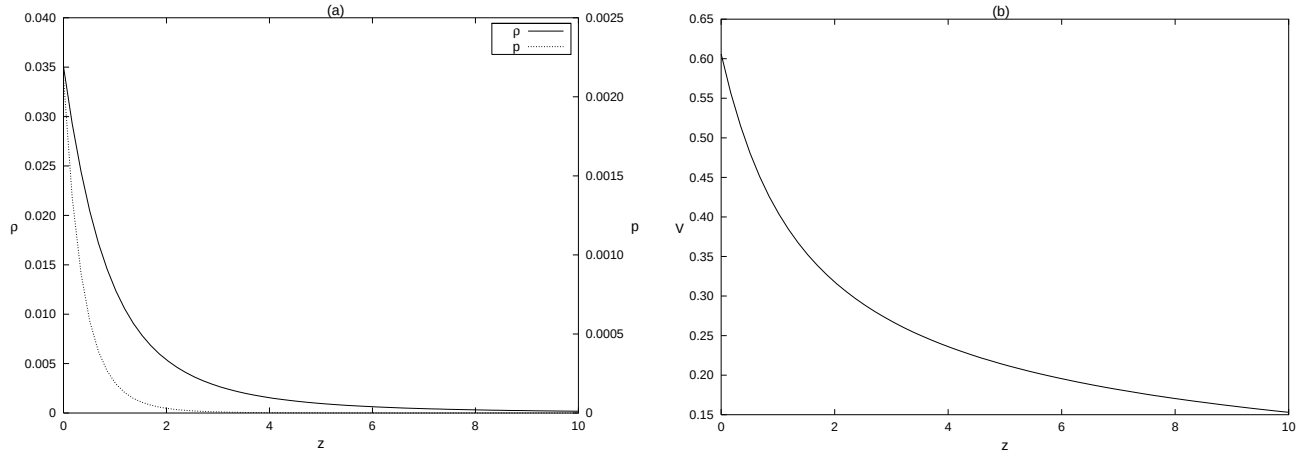

FIG. 7. (a) The density ρ and pressure p [Eq. (25)] and (b) the velocity of sound, V [Eq. (26)] for the halo with $A=0.6; k=1$ and $a=1$ along the z axis.

B. Narlikar-Patwardhan-Vaidya solutions 1a and 1b

Now we shall study the generation of a disk solution with a halo exactly as the one depicted in Fig. 2. We start with a solution of the Einstein equations in isotropic coordinates which represents a sphere with radius r_b of a perfect fluid that on $r=r_b$ will be continuously matched to the vacuum Schwarzschild solution. Narlikar, Patwardhan, and Vaidya (NPV) [24] gave the following two exact solutions of the Einstein equations for perfect fluid static spheres characterized by the metric functions (λ,ν_{1a}) and (λ,ν_{1b}),

$$e^{\lambda}=Cr^{k}, \tag{32}$$

$$e^{\nu_{1a}}=(A_{1a}r^{1-n+k/2}+B_{1a}r^{1+n+k/2})^2 \quad \text{for} \quad -2+\sqrt{2}<k\leqslant 0, \tag{33}$$

$$e^{\nu_{1b}}=r^{\sqrt{2}}[A_{1b}+B_{1b}\ln(r)]^2 \quad \text{for} \quad k=-2+\sqrt{2}, \tag{34}$$

where $A_{1a}, A_{1b}, B_{1a}, B_{1b}$, and C are constants and $n=\sqrt{1+2k+k^2/2}$. We shall refer to these solutions as NPV 1a and NPV 1b, respectively.

The density, pressure, and sound velocity for the solutions (λ,ν_{1a}) and (λ,ν_{1b}) will be denoted by (ρ,p_{1a},V_{1a}) and (ρ,p_{1b},V_{1b}), respectively. We find

$$\rho=\frac{-k(k+4)r^{-2-k}}{32\pi C}, \tag{35}$$

$$p_{1a}=\frac{1}{32\pi Cr^{2+k}(A_{1a}+B_{1a}r^{2n})}\{A_{1a}[3k^2+8(1-n)-4k(n-3)]+B_{1a}[3k^2+8(1+n)+4k(n+3)]r^{2n}\}, \tag{36}$$

$$p_{1b}=\frac{A_{1b}+B_{1b}\ln(r)+2\sqrt{2}B_{1b}}{16\pi C[A_{1b}+B_{1b}\ln(r)]}, \tag{37}$$

$$V_{1a}^2=\frac{1}{k(k+4)(A_{1a}+B_{1a}r^{2n})^2}\{A_{1a}^2[-3k^2+8(n-1)+4k(n-3)]-B_{1a}^2r^{4n}[3k^2+8(1+n)+4k(n+3)]-2A_{1a}B_{1a}r^{2n}[3k(k+4)+8(1-n^2)]\}, \tag{38}$$

$$V_{1b}^2=\frac{2B_{1b}^2r^{\sqrt{2}}}{[A_{1b}+B_{1b}\ln(r)]^2}. \tag{39}$$

The condition of continuity of the metric functions (λ,ν) given by Eqs. (32)–(34) and the corresponding functions in Eq. (9) at the boundary $r=r_b$ leads to the following expressions:

$$\frac{m}{2r_b}=-\frac{k}{k+4}, \quad C=r_b^{-k}\left(\frac{4}{k+4}\right)^4, \tag{40}$$

$$A_{1a}=-\frac{3k^2+8(1+n)+4k(n+3)}{16nr_b^{1-n+k/2}},$$

$$B_{1a}=\frac{3k^2+8(1-n)-4k(n-3)}{16nr_b^{1+n+k/2}}, \tag{41}$$

$$A_{1b}=-\frac{2\sqrt{2}+\ln(r_b)}{4r_b^{1/\sqrt{2}}}, \quad B_{1b}=\frac{1}{4r_b^{1/\sqrt{2}}}. \tag{42}$$

V_{1a} has its maximum at $r=0$ and V_{1b} at $r=r_b$. Condition $V_{1b}(r_b)<1$ is satisfied if $r_b<4^{1/\sqrt{2}}$.

Using Eqs. (32)–(34) in Eqs. (3)–(6), we get the following expressions for the energy density, pressure and sound velocity of the disk:

$$\sigma=-\frac{ka}{4\pi\sqrt{C}\mathcal{R}^{1+k/4}}, \tag{43}$$

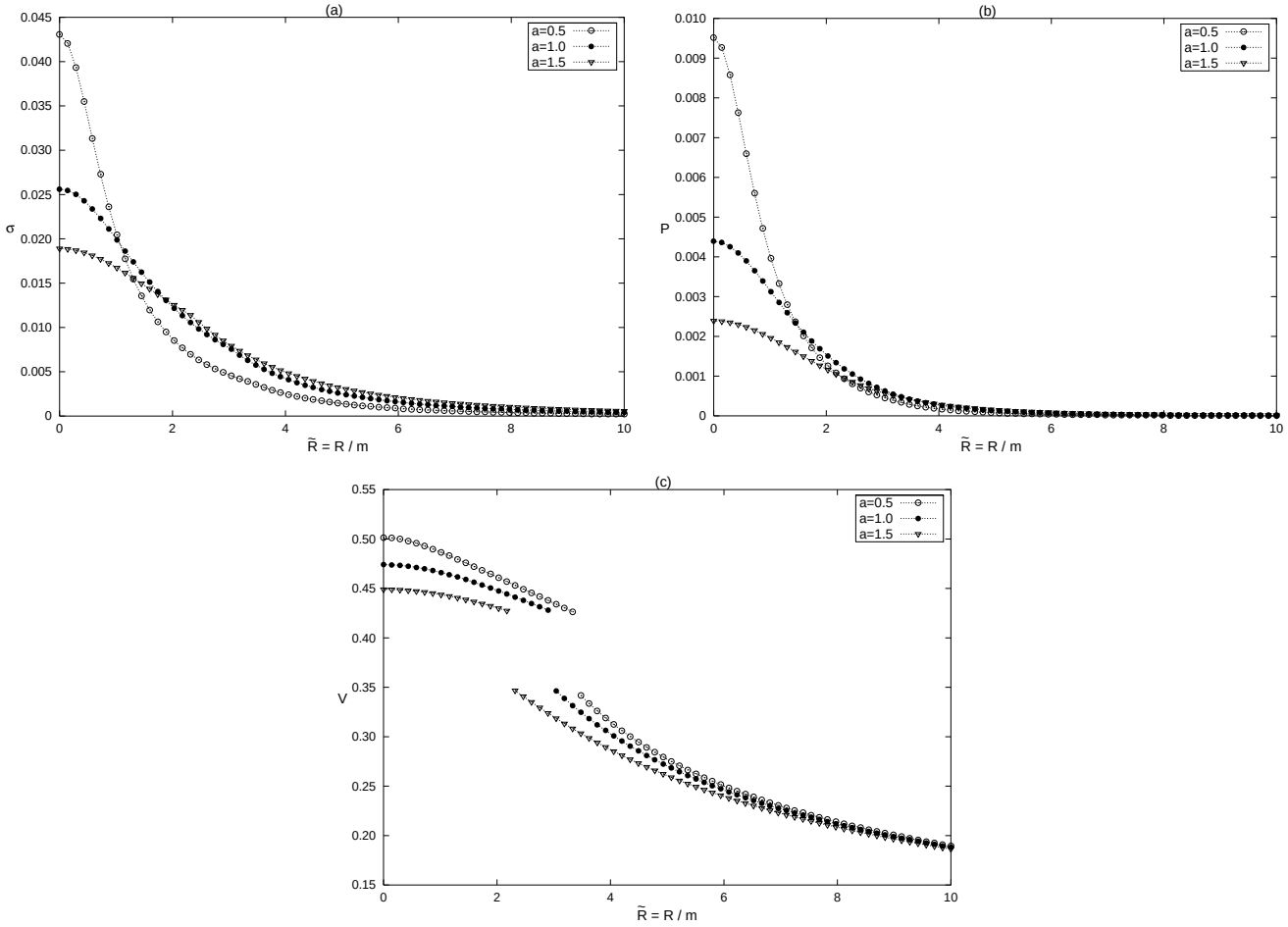

FIG. 8. (a) The surface energy density σ [Eq. (43)], (b) the pressure P [Eq. (44)], and (c) the velocity of sound, V [Eq. (46)] for the disk with $k=-1/2$ and $r_b=2$ for $a=0.5,1.0,$ and 1.5 as functions of $\tilde{R}=R/m$.

$$P_{1a}=\frac{a}{4\pi\sqrt{C}\mathcal{R}^{1+k/4}}\frac{[A_{1a}(k-n+1)+B_{1a}(k+n+1)\mathcal{R}^n]}{[A_{1a}+B_{1a}\mathcal{R}^n]}, \tag{44}$$

$$P_{1b}=\frac{a}{4\pi\sqrt{C}\mathcal{R}^{1/2+\sqrt{2}/4}[2A_{1b}+B_{1b}\ln(\mathcal{R})]}[2A_{1b}(\sqrt{2}-1)+2B_{1b}+B_{1b}(\sqrt{2}-1)\ln(\mathcal{R})], \tag{45}$$

$$V_{1a}^2=\frac{1}{k(k+4)[A_{1a}\mathcal{R}^{-n/2}+B_{1a}\mathcal{R}^{n/2}]^2}[-B_{1a}^2\mathcal{R}^n(k^2+5k+nk+4n+4)+A_{1a}^2\mathcal{R}^{-n}(-k^2-5k+nk+4n-4)+2A_{1a}B_{1a}(-k^2-5k+4n^2-4)], \tag{46}$$

$$V_{1b}^2=\frac{1}{2(2A_{1b}+B_{1b}\ln(\mathcal{R}))^2}[B_{1b}^2\sqrt{2}\ln^2(\mathcal{R})+2B_{1b}(2B_{1b}+B_{1b}\sqrt{2}+2A_{1b}\sqrt{2})\ln(\mathcal{R})+4A_{1b}B_{1b}(2+\sqrt{2})+4\sqrt{2}A_{1b}^2+8B_{1b}^2], \tag{47}$$

where $\mathcal{R}=R^2+a^2$. V_{1a} and V_{1b} have their maximum values at $R=0$. Because the expressions are rather involved, the restrictions on the constants, to ensure that the velocities are positive and less than one, are best made graphically. The curves of σ, P, and V as functions of $\tilde{R}=R/m$ with parameters $k=-1/2;r_b=2$ for $a=0.5,1.0$ and 1.5 are displayed in Figs. 8(a)–8(c), respectively. Figures 9(a)–9(b) show the density ρ, pressure p, and velocity of sound, V for the halo with parameters $k=-1/2;r_b=2$, for $a=0.5$ along the axis z. The same physical quantities are shown in Figs. 10(a)–10(c) and 11(a) and 11(b) with $k=-2+\sqrt{2}$. We note that σ and P are continuous at the boundary between the internal and external parts of the disk, but the velocity of sound has a discontinuity.

The tangential velocity v_c is given by

$$v_{c1a}^2=2R^2\frac{A_{1a}(1-n+k/2)+B_{1a}(1+n+k/2)(R^2+a^2)^n}{[A_{1a}+B_{1a}(R^2+a^2)^n][R^2(k+2)+2a^2]}, \tag{48}$$

$$v_{c1b}^2=R^2\frac{2\sqrt{2}A_{1b}+B_{1b}[4+\sqrt{2}\ln(R^2+a^2)]}{[2A_{1b}+B_{1b}\ln(R^2+a^2)][2a^2+\sqrt{2}R^2]}, \tag{49}$$

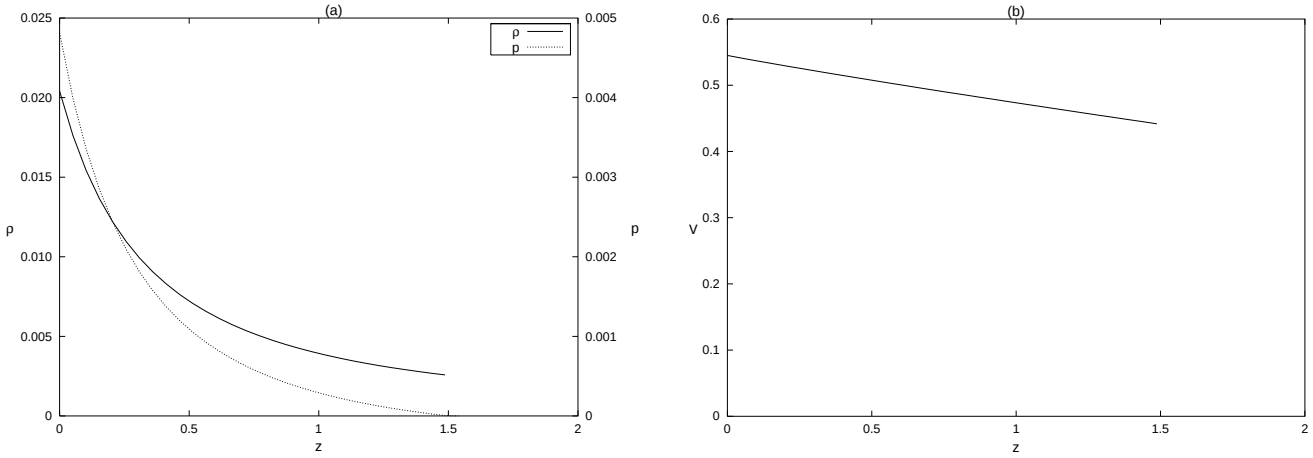

FIG. 9. (a) The density ρ [Eq. (35)] and pressure p [Eq. (36)], and (b) the velocity of sound, V [Eq. (38)] for the halo with $k=-1/2$ and $r_b=2$ for $a=0.5$ along the z axis.

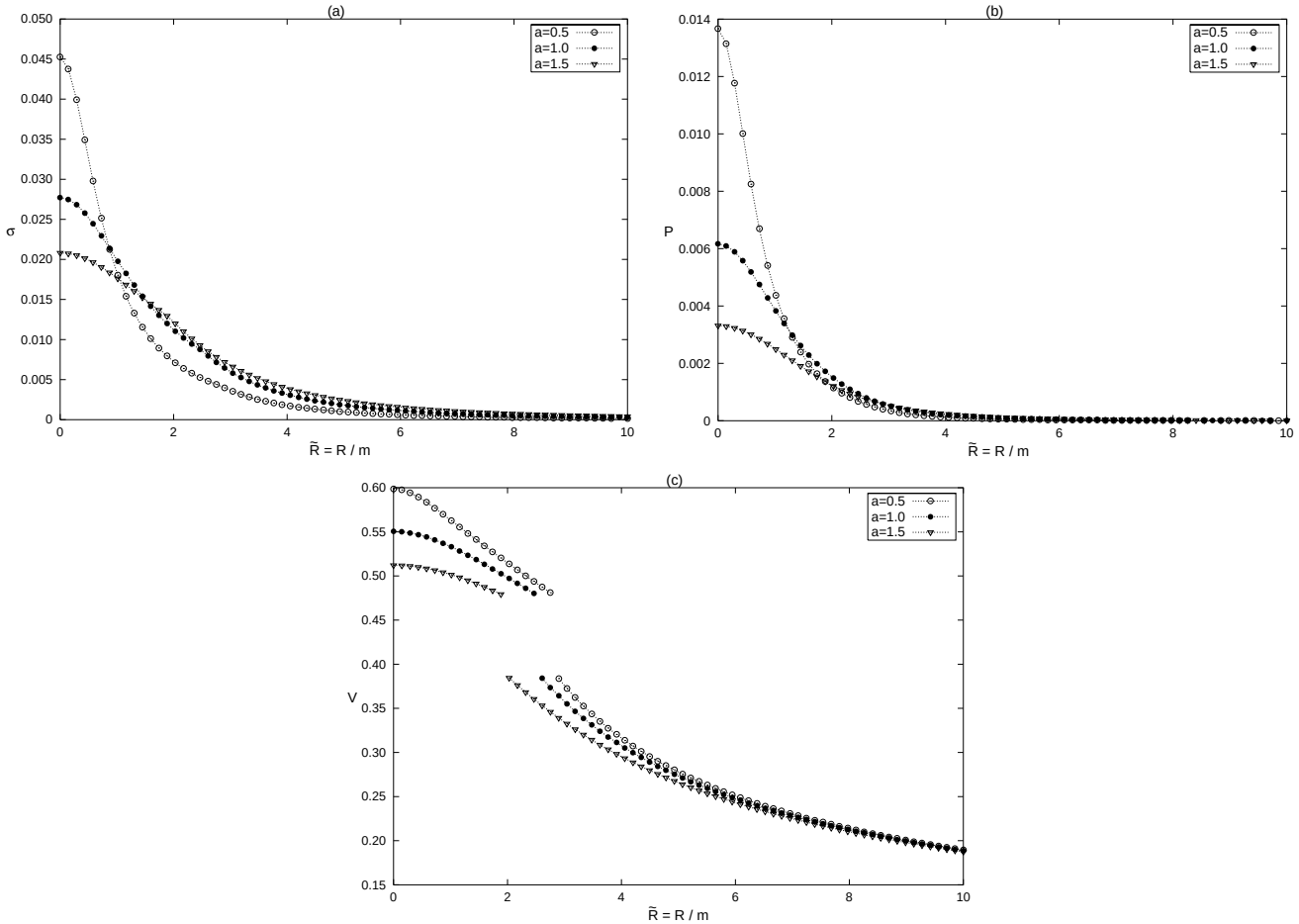

FIG. 10. (a) The surface energy density σ [Eq. (43)], (b) the pressure P [Eq. (45)], and (c) the velocity of sound V [Eq. (47)] for the disk with $k=-2+\sqrt{2}$ and $r_b=2$ for $a=0.5,1.0,$ and 1.5 as functions of $\tilde{R}=R/m$.

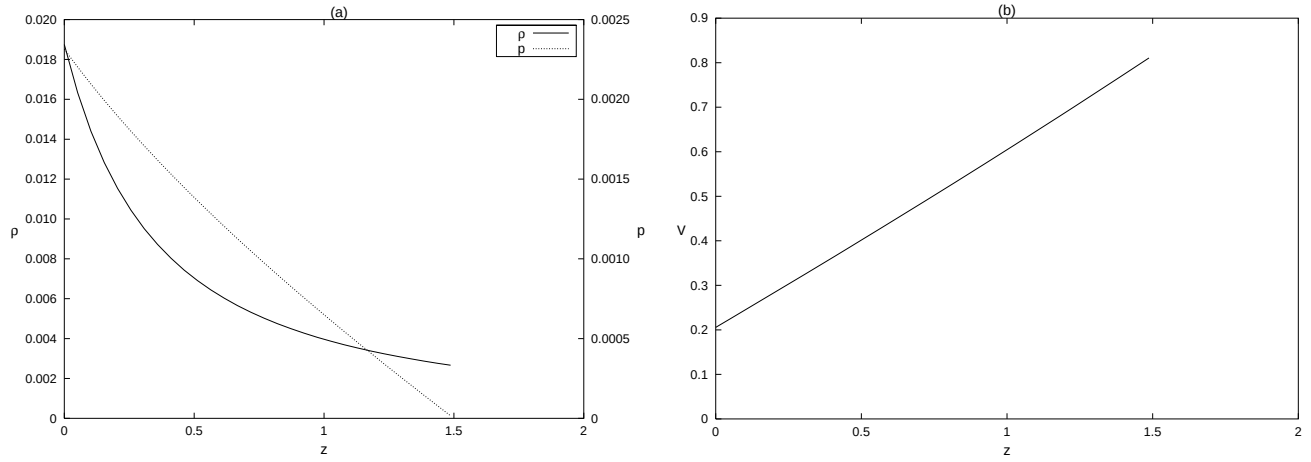

FIG. 11. (a) The density ρ [Eq. (35)] and pressure p [Eq. (37)] and (b) the velocity of sound V [Eq. (39)] for the halo with $k=-2+\sqrt{2}$ and $r_b=2$ for $a=0.5$ along the z axis.

and the specific angular momentum h,

$$h_{1a}=\sqrt{C}R^2(R^2+a^2)^{k/4} \times\sqrt{\frac{A_{1a}(1-n+k/2)+B_{1a}(1+n+k/2)(R^2+a^2)^n}{A_{1a}(a^2+nR^2)+B_{1a}(a^2-nR^2)(R^2+a^2)^n}}, \tag{50}$$

$$h_{1b}=\sqrt{C}R^2(R^2+a^2)^{-1/2+\sqrt{2}/4} \times\sqrt{\frac{2B_{1b}+\sqrt{2}[A_{1b}+B_{1b}\ln(\sqrt{R^2+a^2})]}{2a^2[A_{1b}+B_{1b}\ln(\sqrt{R^2+a^2})]-2B_{1b}R^2}}. \tag{51}$$

In Figs. 12(a) and 12(b), the curves of tangential velocity [Eq. (48)] and $h(dh/d\tilde{R})$ [Eq. (50)], respectively, are displayed as functions of $\tilde{R}=R/m$ with $k=-1/2$ and $r_b=2;a=0.5,1.0$, and 1.5. The same quantities are shown in Figs. 13(a) and 13(b) with $k=-2+\sqrt{2}$. For $a=0.5$ the disks have a small region of unstable orbits immediately after the ''boundary radius.''

C. Narlikar-Patwardhan-Vaidya solutions 2a and 2b

As in the previous sections we study the generation of a disk solution with a halo exactly as the one depicted in Fig. 2. We also start with a solution of the Einstein equations in isotropic coordinates, which represents a sphere of radius r_b of a perfect fluid that on $r=r_b$ will be continuously matched to the vacuum Schwarzschild solution. We will use two other solutions found by Narlikar, Patwardhan, and Vaidya [24] that we shall refer as NPV 2a and NPV 2b, respectively, which are characterized by the metric functions (λ,ν_{2a}) and (λ,ν_{2b}),

$$e^{\lambda}=\frac{1}{(A_1r^{1+n/2}+A_2r^{1-n/2})^2}, \tag{52}$$

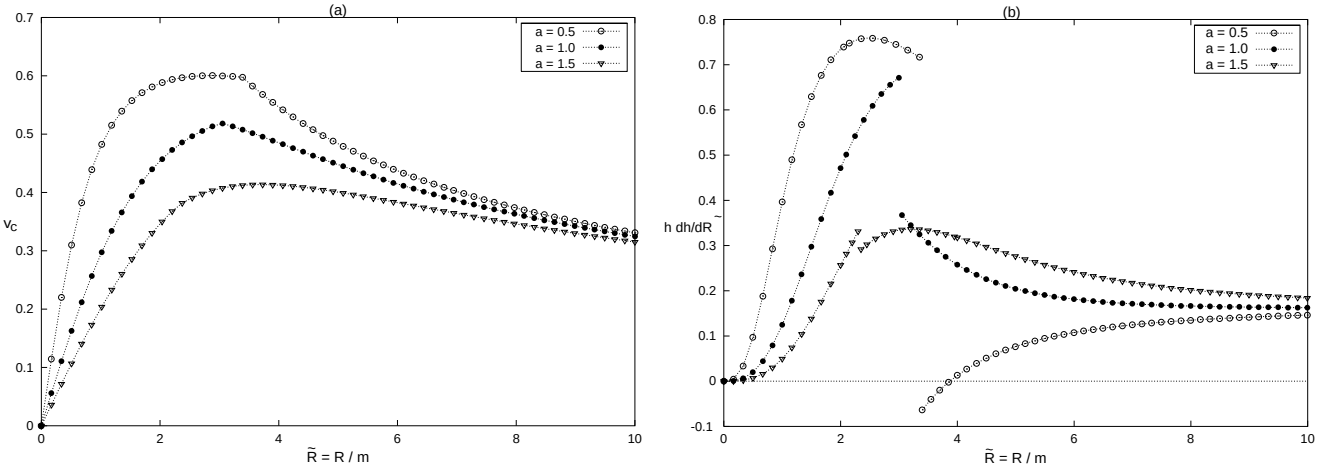

FIG. 12. (a) The tangential velocity v_{c1} [Eq. (48)] and (b) the curves of $h(dh/d\tilde{R})$ [Eq. (50)] with $k=-1/2$ and $r_b=2$ for $a=0.5,1.0$, and 1.5 as functions of $\tilde{R}=R/m$. A region of instability appears on the disk generated with parameter $a=0.5$.

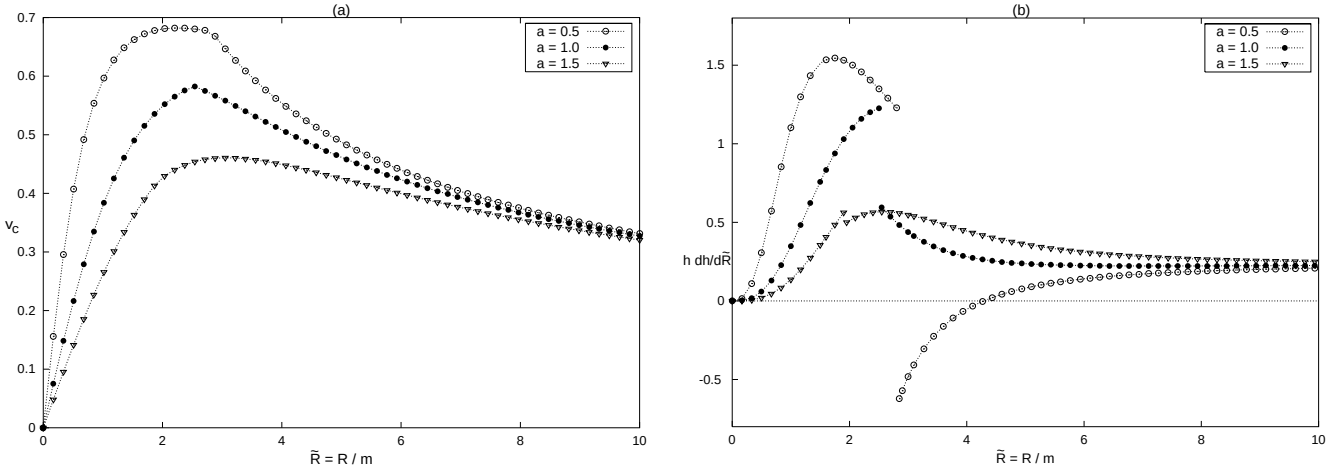

FIG. 13. (a) The tangential velocity v_{c2} [Eq. (49)] and (b) the curves of $h(dh/d\tilde{R})$ [Eq. (51)] with $k=-2+\sqrt{2}$ and $r_b=2$ for $a=0.5$, 1.0, and 1.5 as functions of $\tilde{R}=R/m$. As in the previous case, the same region of instability occurs.

$$e^{\nu_{2a}}=\frac{(B_{1a}r^{1+x/2}+B_{2a}r^{1-x/2})^2}{(A_1r^{1+n/2}+A_2r^{1-n/2})^2} \quad \text{for} \quad \sqrt{2}<n\leqslant 2, \tag{53}$$

$$e^{\nu_{2b}}=\frac{[B_{1b}+B_{2b}\ln(r)]^2}{(A_1r^{1/\sqrt{2}}+A_2r^{-1/\sqrt{2}})^2} \quad \text{for} \quad n=\sqrt{2}, \tag{54}$$

where the A's and B's are constants and $x=\sqrt{2n^2-4}$. The solution (λ,ν_{2a}) with $n=2$ corresponds to Schwarzschild's internal solution in isotropic coordinates (see, for instance, Ref. [22]). This solution has constant density and is conformally flat when $B_{1a}=0$.

The density, pressure, and sound velocity for the solutions (λ,ν_{2a}) and (λ,ν_{2b}) will be denoted by (ρ,p_{2a},V_{2a}) and (ρ,p_{2b},V_{2b}), respectively. We find

$$\rho=\frac{1}{32\pi}[(4-n^2)(A_1r^{n/2}+A_2r^{-n/2})^2+12n^2A_1A_2], \tag{55}$$

$$p_{2a}=\frac{1}{32\pi}\left[-12n^2A_1A_2+(3n^2-4)(A_1r^{n/2}+A_2r^{-n/2})^2+\frac{2nx(B_{2a}-B_{1a}r^x)}{B_{2a}+B_{1a}r^x}(A_1^2r^n-A_2^2r^{-n})\right], \tag{56}$$

$$p_{2b}=\frac{1}{16\pi[B_{1b}+B_{2b}\ln(r)]}\{[B_{1b}+B_{2b}\ln(r)](A_1^2r^{\sqrt{2}}+A_2^2r^{-\sqrt{2}}-10A_1A_2)+2\sqrt{2}B_{2b}(A_2^2r^{-\sqrt{2}}-A_1^2r^{\sqrt{2}})\}, \tag{57}$$

$$V_{2a}^2=\frac{1}{(4-n^2)(A_1^2r^n-A_2^2r^{-n})(B_{2a}+B_{1a}r^x)^2}\times\{B_{2a}^2[A_1^2r^n(3n^2+2nx-4)+A_2^2r^{-n}\times(-3n^2+2nx+4)]+B_{1a}^2r^{2x}[A_1^2r^n(3n^2-2nx-4)+A_2^2r^{-n}(-3n^2-2nx+4)]+2B_{1a}B_{2a}r^x\times[A_1^2r^n(3n^2-2x^2-4)+A_2^2r^{-n}(-3n^2+2x^2+4)]\}, \tag{58}$$

$$V_{2b}^2=\frac{1}{[B_{1b}+B_{2b}\ln(r)]^2(A_1^2r^{\sqrt{2}}-A_2^2r^{-\sqrt{2}})}\times(A_1^2r^{\sqrt{2}}\{[B_{1b}+B_{2b}\ln(r)][B_{1b}+B_{2b}\ln(r)-2\sqrt{2}B_{2b}]+2B_{2b}^2\}-A_2^2r^{-\sqrt{2}}\{[B_{1b}+B_{2b}\ln(r)][B_{1b}+B_{2b}\ln(r)+2\sqrt{2}B_{2b}]+2B_{2b}^2\}). \tag{59}$$

The condition of continuity of the metric functions (λ,ν) given by Eqs. (52)–(54) and the corresponding functions in Eq. (9) at the boundary $r=r_b$ leads to the following expressions:

$$A_1=\frac{1}{nr_b^{2+n/2}\left(1+\frac{m}{2r_b}\right)^3}\left[\frac{m}{2}-r_b\left(1-\frac{n}{2}-\frac{mn}{4r_b}\right)\right], \tag{60}$$

$$A_2=\frac{1}{r_b^{2-n/2}\left(1+\frac{m}{2r_b}\right)^3}\left[-\frac{m}{2n}+r_b\left(\frac{1}{2}+\frac{1}{n}+\frac{m}{4r_b}\right)\right], \tag{61}$$

$$B_{1a}=\frac{-4r_b^2\left(1-\frac{2m}{r_b}\right)-m^2+2xr_b^2\left(1-\frac{m^2}{4r_b^2}\right)}{4xr_b^{3+x/2}\left(1+\frac{m}{2r_b}\right)^4}, \tag{62}$$

$$B_{2a}=\frac{4r_b^2\left(1-\frac{2m}{r_b}\right)+m^2+2xr_b^2\left(1-\frac{m^2}{4r_b^2}\right)}{4xr_b^{3-x/2}\left(1+\frac{m}{2r_b}\right)^4}, \tag{63}$$

$$B_{1b}=\frac{1}{4r_b^3\left(1+\frac{m}{2r_b}\right)^4}[4r_b^2-m^2 +(m^2-8mr_b+4r_b^2)\ln(r_b)], \tag{64}$$

$$B_{2b}=-\frac{m^2-8mr_b+4r_b^2}{4r_b^3\left(1+\frac{m}{2r_b}\right)^4}. \tag{65}$$

V_{2a} has its maximum at $r=r_b$, and V_{2b} at $r=0$.

Using Eqs. (52)–(54) in Eqs. (3)–(6), we get the expressions for the energy density, pressure, and sound velocity of the disk:

$$\sigma=\frac{a}{4\pi}[A_1(2+n)\mathcal{R}^{-1/2+n/4}+A_2(2-n)\mathcal{R}^{-1/2-n/4}], \tag{66}$$

$$\begin{aligned}P_{2a}=&-\frac{a}{8\pi(B_{1a}\mathcal{R}^{1/2+x/4}+B_{2a}\mathcal{R}^{1/2-x/4})}[B_{1a}A_1(2+2n\\&-x)\mathcal{R}^{(x+n)/4}+B_{1a}A_2(2-2n-x)\mathcal{R}^{(x-n)/4}\\&+B_{2a}A_1(2+2n+x)\mathcal{R}^{(-x+n)/4}\\&+B_{2a}A_2(2-2n+x)\mathcal{R}^{-(x+n)/4}],\end{aligned} \tag{67}$$

$$\begin{aligned}P_{2b}=&-\frac{a}{4\pi[2B_{1b}+B_{2b}\ln(\mathcal{R})]}\{2(1+\sqrt{2})B_{1b}A_1\\&\times\mathcal{R}^{-1/2+\sqrt{2}/4}+2(1-\sqrt{2})B_{1b}A_2\mathcal{R}^{-1/2-\sqrt{2}/4}\\&+[(1+\sqrt{2})\ln(\mathcal{R})-2]B_{2b}A_1\mathcal{R}^{-1/2+\sqrt{2}/4}\\&+[(1-\sqrt{2})\ln(\mathcal{R})-2]B_{2b}A_2\mathcal{R}^{-1/2-\sqrt{2}/4}\},\end{aligned} \tag{68}$$

$$\begin{aligned}V_{2a}^2=&\frac{1}{2(4-n^2)[A_2+A_1\mathcal{R}^{n/2}][B_{2a}+B_{1a}\mathcal{R}^{x/2}]^2}\\&\times\{A_1\mathcal{R}^{n/2}[B_{1a}^2(n-2)(2n-x+2)\mathcal{R}^x+B_{2a}^2(n-2)\\&\times(2n+x+2)-4B_{1a}B_{2a}(-n^2+n+x^2+2)\mathcal{R}^{x/2}]\\&+A_2[B_{1a}^2(n+2)(2n+x-2)\mathcal{R}^x+B_{2a}^2(n+2)\\&\times(2n-x-2)-4B_{1a}B_{2a}\\&\times(-n^2-n+x^2+2)\mathcal{R}^{x/2}]\},\end{aligned} \tag{69}$$

$$\begin{aligned}V_{2b}^2=&-\frac{2B_{1b}+2B_{2b}+B_{2b}\ln(\mathcal{R})}{2[2B_{1b}+B_{2b}\ln(\mathcal{R})]^2[A_2+A_1\mathcal{R}^{1/\sqrt{2}}]}\{[\sqrt{2}\ln(\mathcal{R})\\&-4]B_{2b}A_1\mathcal{R}^{1/\sqrt{2}}-[\sqrt{2}\ln(\mathcal{R})+4]B_{2b}A_2\\&+2\sqrt{2}B_{1b}[A_1\mathcal{R}^{1/\sqrt{2}}-A_2]\},\end{aligned} \tag{70}$$

where $\mathcal{R}=R^2+a^2$. The curves of σ, P, and V as functions of $\tilde{R}=R/m$ with parameters $n=1.8$,$m=0.5$, and $r_b=2$ for $a=0.5$,1.0, and 1.5 are displayed in Figs. 14(a)–14(c), respectively. Figures 15(a)–15(b) show the density ρ, pressure p, and velocity of sound, V for the halo with parameters $n=1.8$, $m=0.5$, $r_b=2$, for $a=0.5$ along the z axis. The same physical quantities are shown in Figs. 16 and 17 with $n=\sqrt{2}$.

The tangential velocity v_c is given by

$$v_{c2a}^2=R^2\frac{A_2[B_{1a}(n+x)\mathcal{R}^{x/2}+B_{2a}(n-x)]-A_1\mathcal{R}^{n/2}[B_{1a}(n-x)\mathcal{R}^{x/2}+B_{2a}(n+x)]}{[B_{1a}\mathcal{R}^{x/2}+B_{2a}][A_1\mathcal{R}^{n/2}(2a^2-nR^2)+A_2(2a^2+nR^2)]}, \tag{71}$$

$$v_{c2b}^2=R^2\frac{A_2\{2\sqrt{2}B_{1b}+B_{2b}[4+\sqrt{2}\ln(\mathcal{R})]\}-A_1\mathcal{R}^{\sqrt{2}/2}\{2\sqrt{2}B_{1b}+B_{2b}[-4+\sqrt{2}\ln(\mathcal{R})]\}}{[2B_{1b}+B_{2b}\ln(\mathcal{R})][A_1\mathcal{R}^{\sqrt{2}/2}(2a^2-\sqrt{2}R^2)+A_2(2a^2+\sqrt{2}R^2)]}, \tag{72}$$

and the specific angular momentum h

$$\begin{aligned}h_{2a}=&\frac{R^2\mathcal{R}^{-1/2+n/4}}{(A_1\mathcal{R}^{n/2}+A_2)^{3/2}\sqrt{B_{1a}(2a^2-xR^2)\mathcal{R}^{x/2}+B_{2a}(2a^2+xR^2)}}\{A_2[B_{1a}(n+x)\mathcal{R}^{x/2}+B_{2a}(n-x)]\\&-A_1\mathcal{R}^{n/2}[B_{1a}(n-x)\mathcal{R}^{x/2}+B_{2a}(n+x)]\}^{1/2},\end{aligned} \tag{73}$$

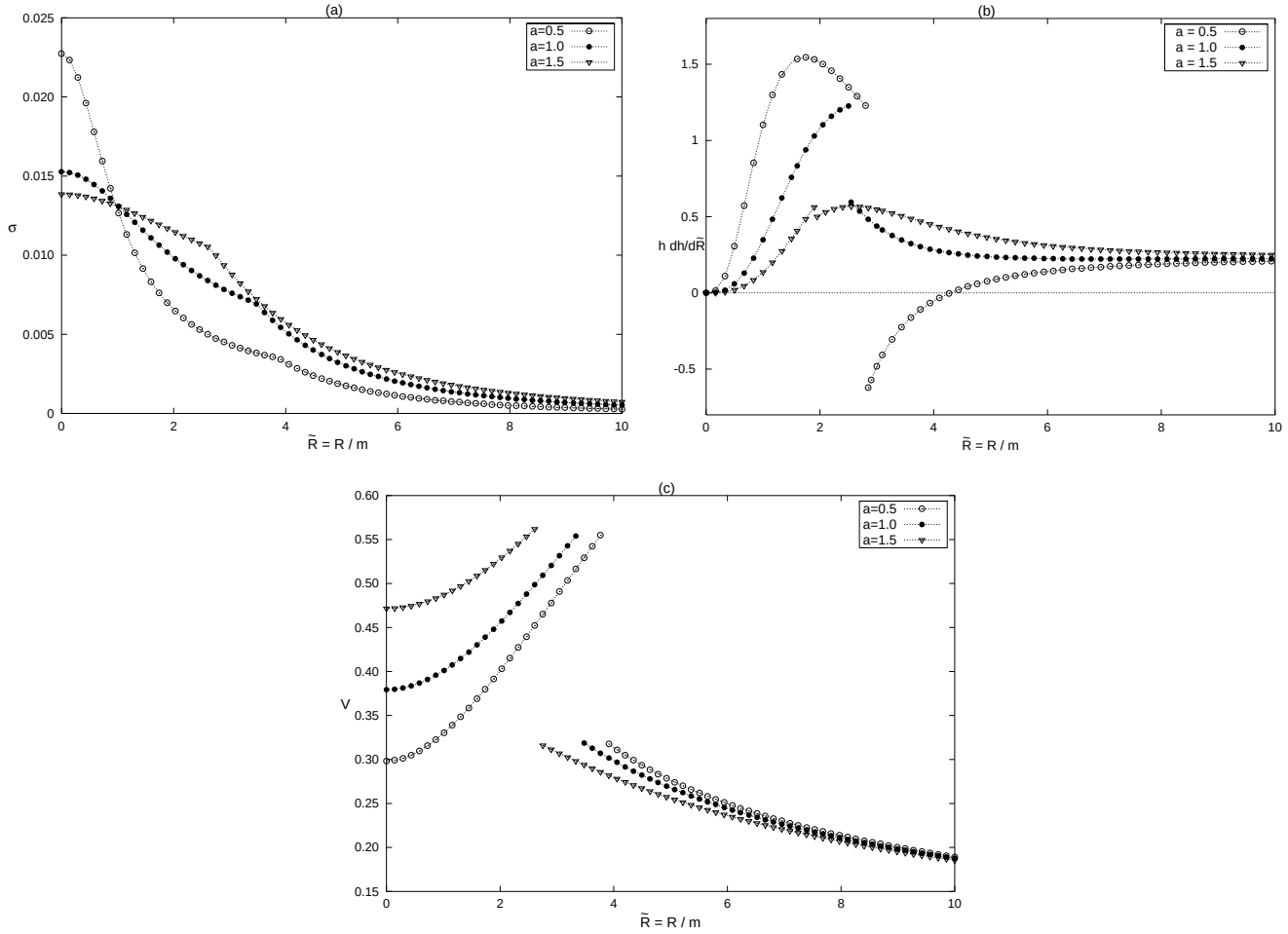

FIG. 14. (a) The surface energy density σ [Eq. (66)], (b) the pressure P [Eq. (67)], and (c) the velocity of sound, V [Eq. (69)], for the disk with $n=1.8; m=0.5,$ and $r_b=2$ for $a=0.5,1.0$ and 1.5 as functions of $\tilde{R}=R/m$.

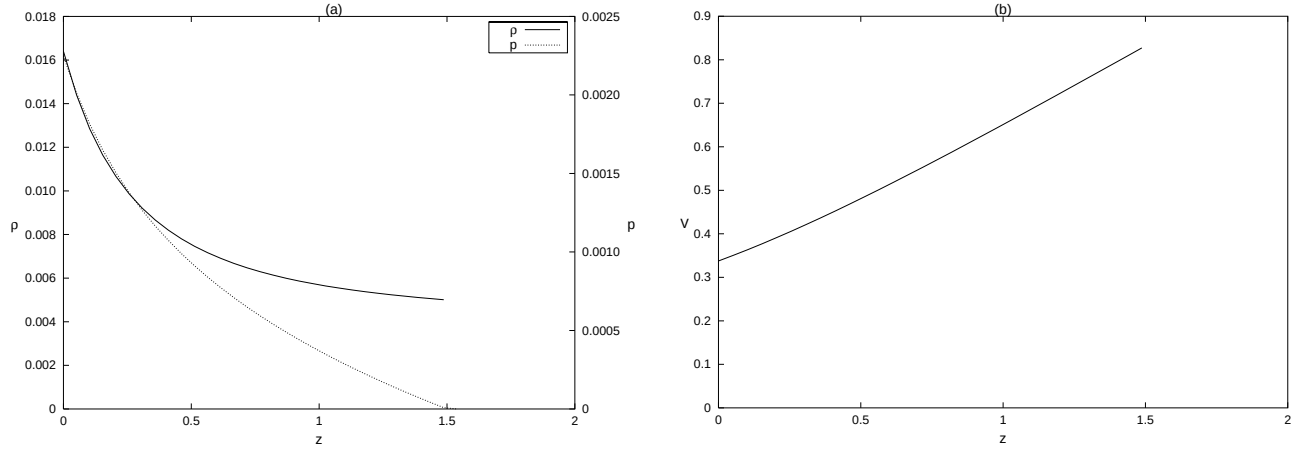

FIG. 15. (a) The density ρ [Eq. (55)] and pressure p [Eq. (56)], and (b) the velocity of sound, V [Eq. (58)] for the halo with $n=1.8. m=0.5,$ and $r_b=2$ for $a=0.5$ along the z axis.

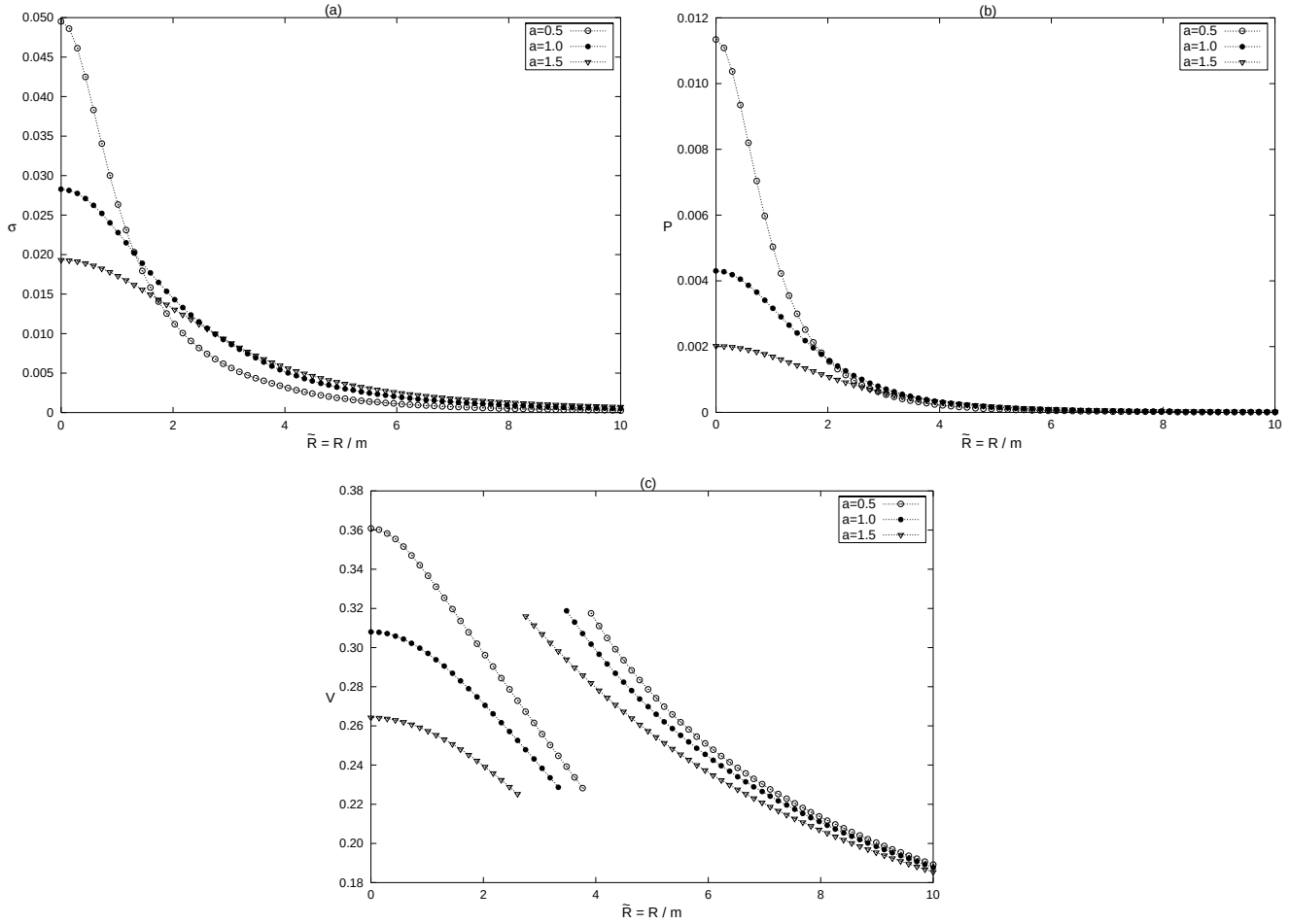

FIG. 16. (a) The surface energy density σ [Eq. (66)], (b) the pressure P [Eq. (68)], and (c) the velocity of sound, V [Eq. (70)], for the disk with $n=\sqrt{2}, r_b=2,$ and $m=0.5$ for $a=0.5,1.0,$ and 1.5 as functions of $\tilde{R}=R/m$.

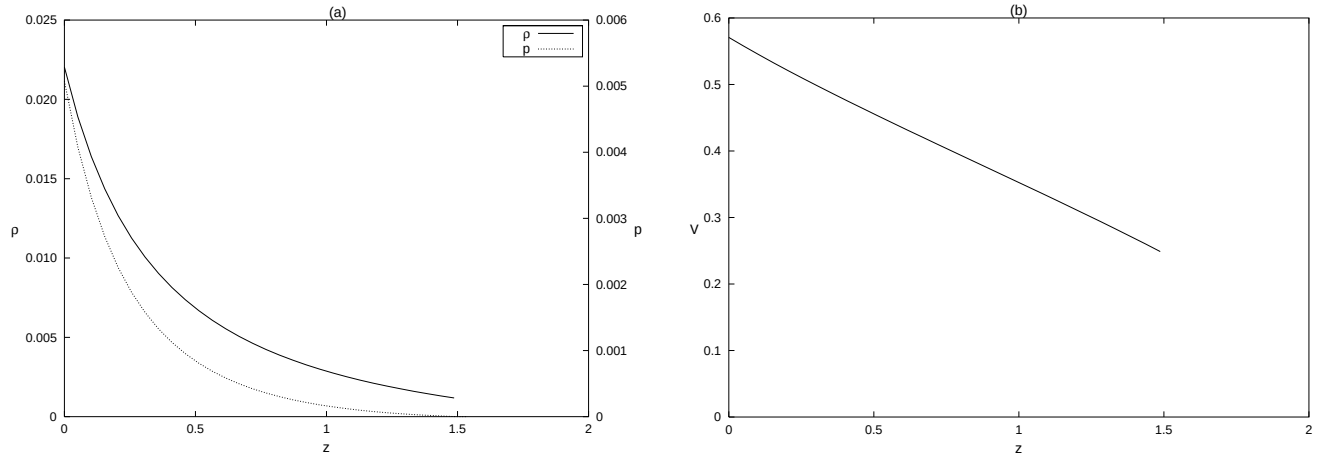

FIG. 17. (a) The density ρ [Eq. (55)] and pressure p [Eq. (57)], and (b) the velocity of sound, V [Eq. (59)] for the halo with $n=\sqrt{2}$ and $r_b=2$ for $a=0.5$ along the z axis.

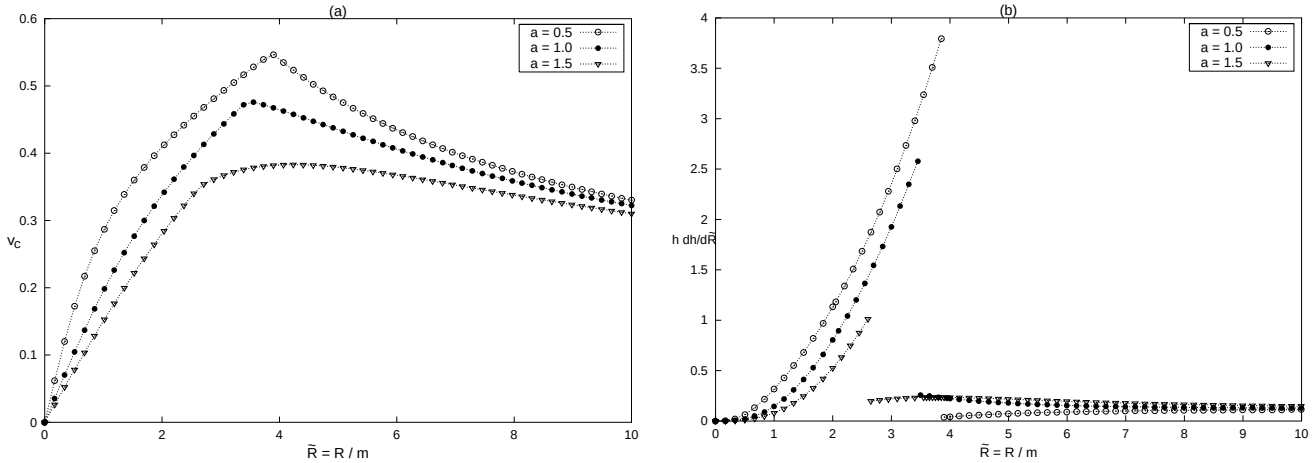

FIG. 18. (a) The tangential velocity v_{ca} [Eq. (71)], and (b) the curves of $hdh/d\tilde{R}$ [Eq. (73)] with $n=1.8$,$m=0.5$ and $r_b=2$ for $a=0.5$, 1.0, and 1.5 as functions of $\tilde{R}=R/m$. The disks have no unstable orbits for these parameters.

$$h_{2b}=\frac{R^2\mathcal{R}^{-1/2+\sqrt{2}/4}}{[A_1\mathcal{R}^{\sqrt{2}/2}+A_2]^{3/2}\sqrt{4a^2B_{1b}+2B_{2b}[-2R^2+a^2\ln(\mathcal{R})]}}(A_2\{2\sqrt{2}B_{1b}+B_{2b}[4+\sqrt{2}\ln(\mathcal{R})]\}$$
$$-A_1\mathcal{R}^{\sqrt{2}/2}\{2\sqrt{2}B_{1b}+B_{2b}[-4+\sqrt{2}\ln(\mathcal{R})]\})^{1/2}. \quad (74)$$

In Figs. 18(a) and 18(b), the curves of tangential velocities, Eq. (71), and $hdh/d\tilde{R}$, Eq. (73), respectively, are displayed as functions of $\tilde{R}=R/m$ with $n=1.8$, $m=0.5$, and $r_b=2$ for $a=0.5$, 1.0, 1.5. Figure 19 shows the same quantities with $n=\sqrt{2}$. Unlike solution 2, no unstable circular orbits are present for the disks constructed with these parameters.

V. DISKS WITH COMPOSITE HALOS FROM SPHERICAL SOLUTIONS

We study two examples of disks with halos constructed from spheres of fluids with two layers as the ones depicted in Fig. 3.

A. Internal Schwarzschild solution and Buchdahl solution

Let us consider that a fluid sphere is formed by two layers: The internal layer, $0\leqslant r<r_1$, will be taken as the internal Schwarzschild solution (solution $2a$ with $n=2$),

$$e^{\nu}=\frac{(B_1r^2+B_2)^2}{(A_1r^2+A_2)^2},\quad e^{\lambda}=\frac{1}{(A_1r^2+A_2)^2}. \quad (75)$$

The external layer, $r>r_1$ is taken as the Buchdahl solution,

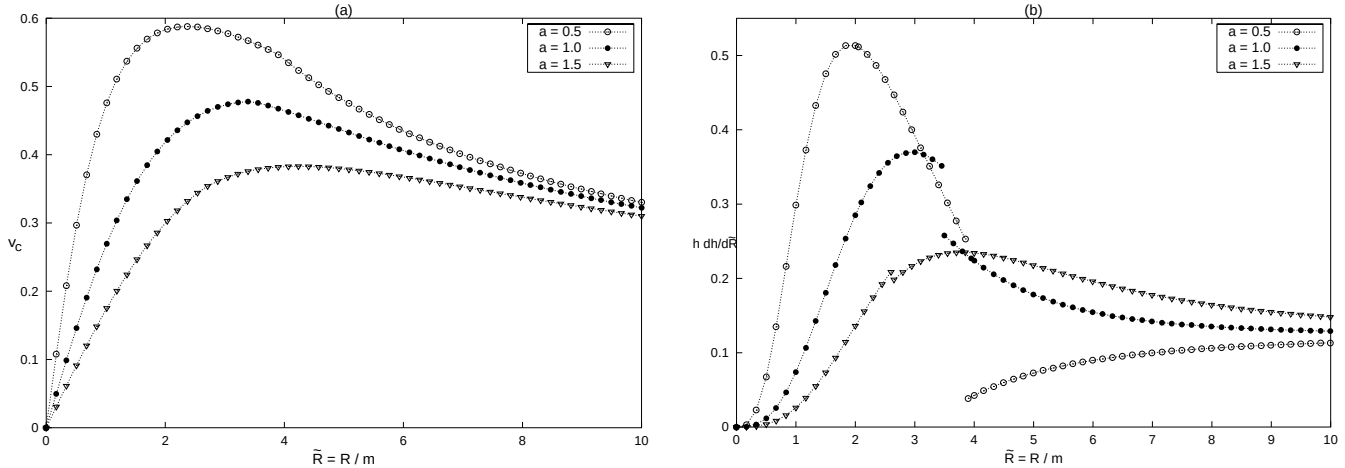

FIG. 19. (a) The tangential velocity v_{cb} [Eq. (72)] and (b) the curves of $hdh/d\tilde{R}$ [Eq. (74)] with $n=\sqrt{2}$, $m=0.5$, and $r_b=2$ for $a=0.5$,1.0, and 1.5 as functions of $\tilde{R}=R/m$. The disks have no unstable orbits for these parameters.

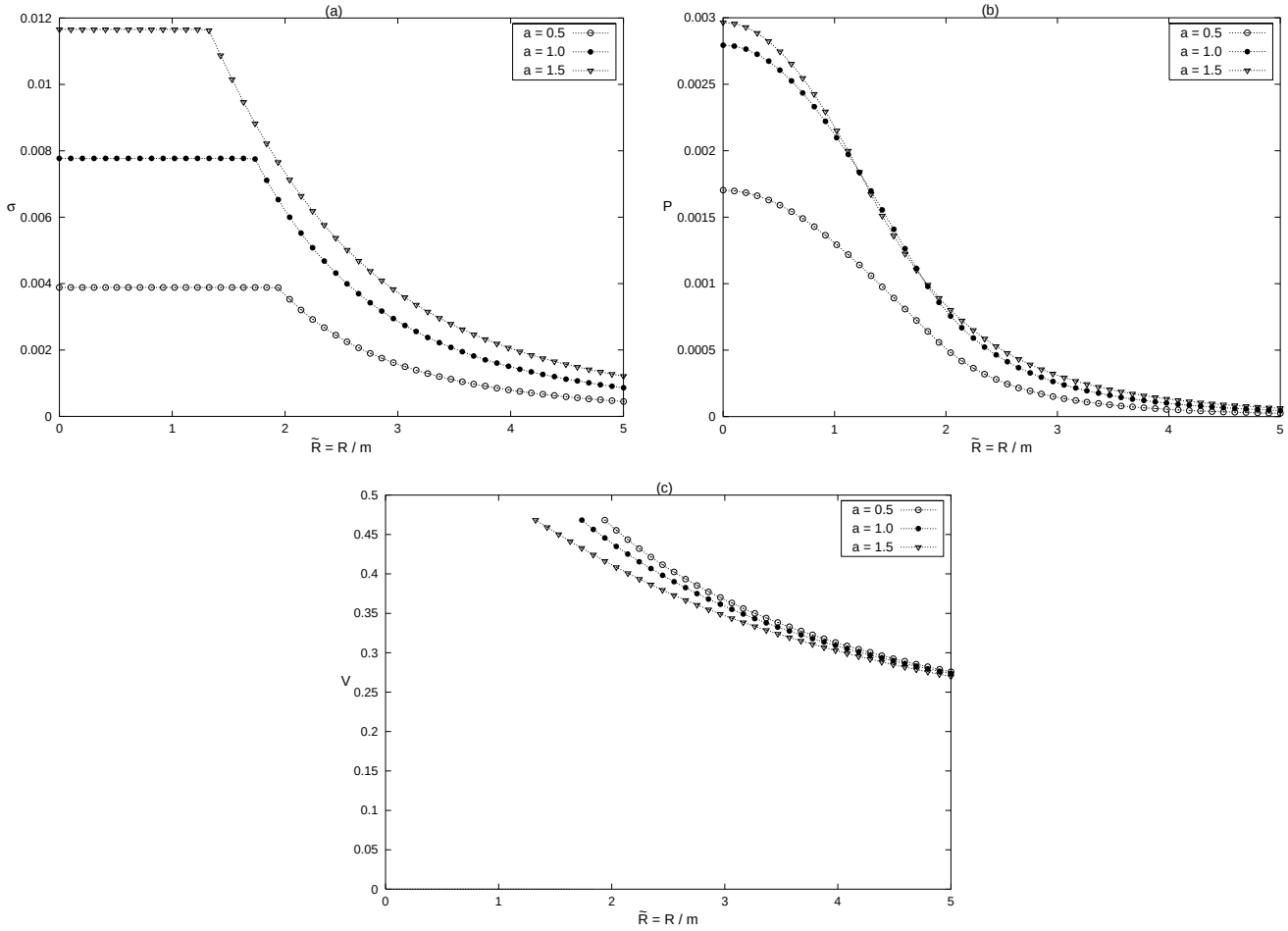

FIG. 20. (a) The surface energy density σ, (b) the pressure P, and (c) the velocity of sound V, for the disk generated from spherical fluid layers Eqs. (75) and (76) with $m=1; k=1$, $r_1=2$, for $a=0.5$, 1.0, and 1.5 as functions of $\tilde{R}=R/m$.

$$e^{\nu}=\left(\frac{1-\frac{C}{\sqrt{1+kr^2}}}{1+\frac{C}{\sqrt{1+kr^2}}}\right)^2, \quad e^{\lambda}=\left(1+\frac{C}{\sqrt{1+kr^2}}\right)^4. \tag{76}$$

Note that the external layer has no boundary, i.e., this layer has infinite radius.

According to the continuity conditions at $r=r_1$, the constants are related through

$$A_1=\frac{Ck}{(C+\sqrt{1+kr_1^2})^3}, \quad A_2=\frac{1+\frac{C}{(1+kr_1^2)^{3/2}}}{\left(1+\frac{C}{\sqrt{1+kr_1^2}}\right)^3}, \tag{77}$$

$$B_1=\frac{Ck}{(1+kr_1^2)\left(1+\frac{C}{\sqrt{1+kr_1^2}}\right)^3}D, \tag{78}$$

$$D=\frac{\left[C(1-3kr_1^2)-\frac{C^2}{\sqrt{1+kr_1^2}}(1-kr_1^2)+2(1+kr_1^2)^{3/2}\right]}{[(1+kr_1^2)^2+2C\sqrt{1+kr_1^2}+C^2(1-kr_1^2)]}, \tag{79}$$

$$B_2=\frac{1-\frac{C}{\sqrt{1+kr_1^2}}}{\left(1+\frac{C}{\sqrt{1+kr_1^2}}\right)^3}-B_1r_1^2. \tag{80}$$

With these relations, one verifies that, using Eqs. (27) and (66), Eqs. (28) and (67), both the energy density and the pressure are continuous at the radius $R=\sqrt{r_1^2-a^2}$ of the disk.

Figures 20(a)–20(c) show respectively, σ, P, and V for the disk obtained from fluid layers, Eq. (75) and (76), with parameters $m=1, k=1$, and $r_1=2$; for $a=0.5, 1.0$, and 1.5 as functions of $\tilde{R}=R/m$. The density ρ, pressure p, and velocity of sound, V, for the halo along the z axis with the same parameters for $a=0.5$ are shown in Fig. 21.

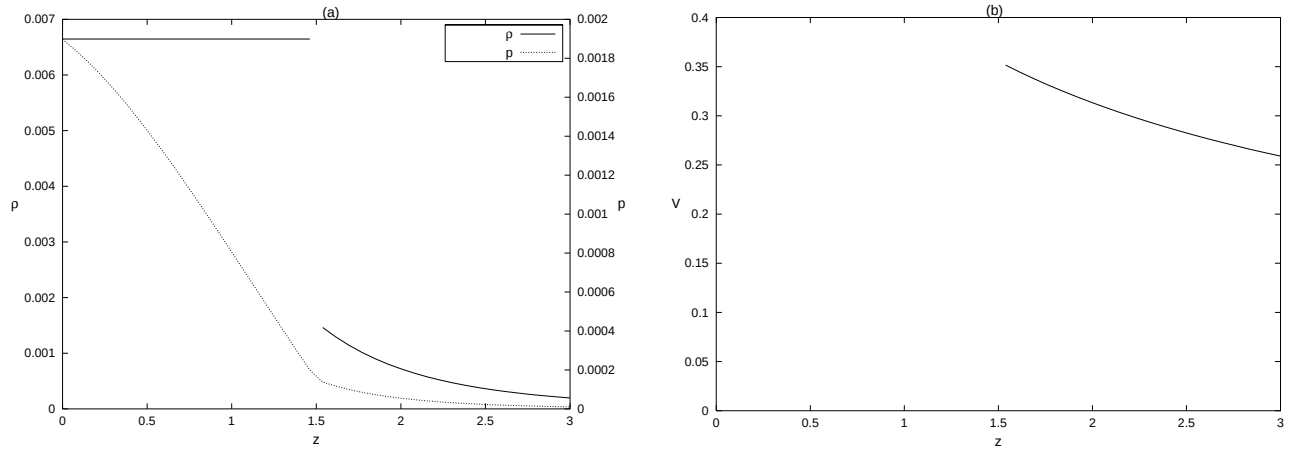

FIG. 21. (a) The density ρ and pressure p and (b) the velocity of sound, V, for the halo formed by fluid layers, Eqs. (75) and (76), with $m=1$, $k=1$, and $r_1=2$, for $a=0.5$ along the z axis.

In Figs. 22(a) and 22(b), the curves of tangential velocities and of $hdh/d\tilde{R}$, respectively, are displayed as functions of $\tilde{R}=R/m$.

B. NPV Solution 2b with $n=\sqrt{2}$ and NPV solution 1b with $k=-2+\sqrt{2}$

Now we consider a sphere composed of two finite layers: The internal layer, $0\leqslant r<r_1$, is taken as the NPV solution 2b with $n=\sqrt{2}$,

$$e^{\nu}=\frac{(B_1+B_2\ln(r))^2}{(A_1r^{\sqrt{2}/2}+A_2r^{-\sqrt{2}/2})^2},\quad e^{\lambda}=\frac{1}{(A_1r^{1+\sqrt{2}/2}+A_2r^{1-\sqrt{2}/2})^2}. \tag{81}$$

The external layer, $r_1<r<r_2$, is taken as the NPV solution 1b with $k=-2+\sqrt{2}$,

$$e^{\nu}=r^{\sqrt{2}}[A_3+B_3\ln(r)]^2,\quad e^{\lambda}=Cr^{-2+\sqrt{2}}. \tag{82}$$

The spacetime outside the sphere, $r>r_2$, will be taken as Schwarzschild's vacuum solution in isotropic coordinates:

$$e^{\nu}=\frac{\left(1-\frac{m}{2r}\right)^2}{\left(1+\frac{m}{2r}\right)^2},\quad e^{\lambda}=\left(1+\frac{m}{2r}\right)^4. \tag{83}$$

In this case the pressure should be zero at $r=r_2$. The continuity conditions at $r=r_1$ and $r=r_2$ give the relations

$$\frac{m}{r_2}=\frac{\sqrt{2}(2-\sqrt{2})}{1+\sqrt{2}},\quad C=\frac{64r_2^{2-\sqrt{2}}}{(1+\sqrt{2})^4},$$

$$B_3=\frac{1}{4r_2^{1/\sqrt{2}}},\quad A_3=-\frac{2\sqrt{2}+\ln(r_2)}{r_2^{1/\sqrt{2}}}, \tag{84}$$

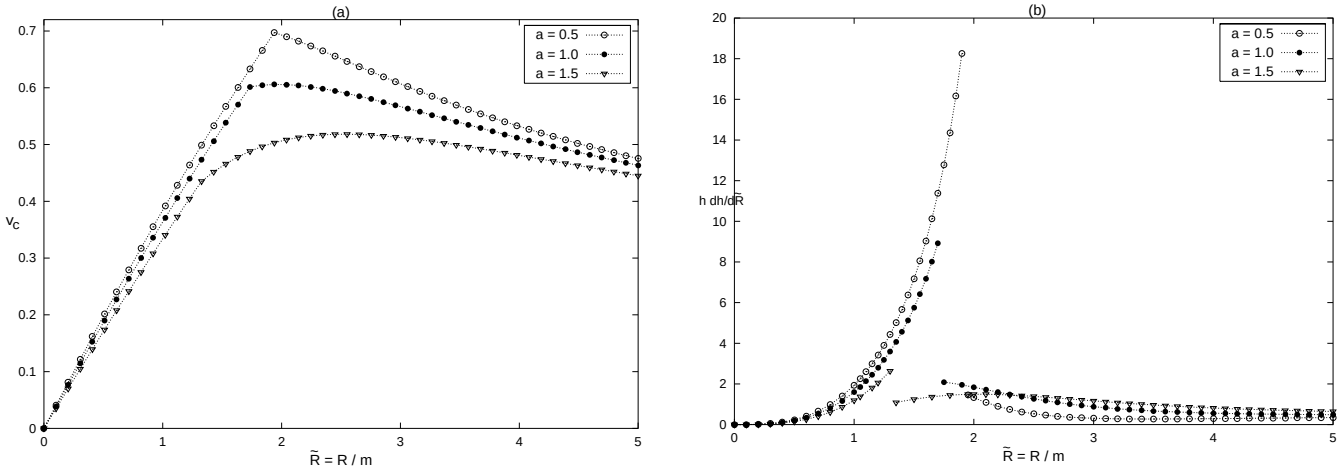

FIG. 22. (a) The tangential velocity v_c and (b) the curves of $hdh/d\tilde{R}$ for the disk generated from fluid layers, Eqs. (75) and (76), with $m=1$, $k=1$, and $r_1=2$ for $a=0.5$, 1.0, and 1.5 as functions of $\tilde{R}=R/m$. The disks obtained with these parameters have no unstable orbits.

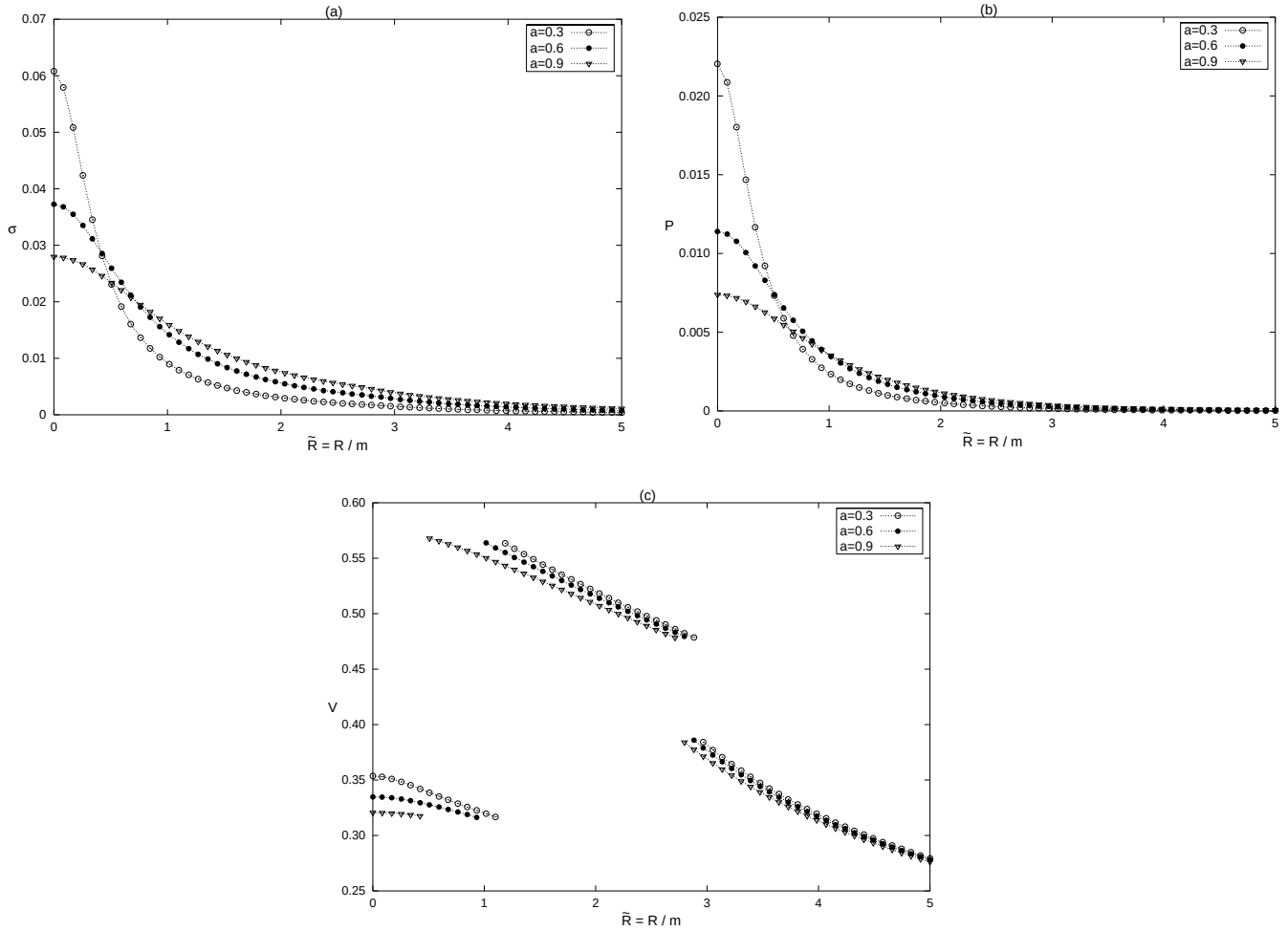

FIG. 23. (a) The surface energy density σ, (b) the pressure P, and (c) the velocity of sound, V, for the disk generated from spherical fluid layers, Eqs. (81) and (82), with $r_1=1$ and $r_2=2$ for $a=0.3,\ 0.6$ and 0.9 as function of $\tilde{R}=R/m$.

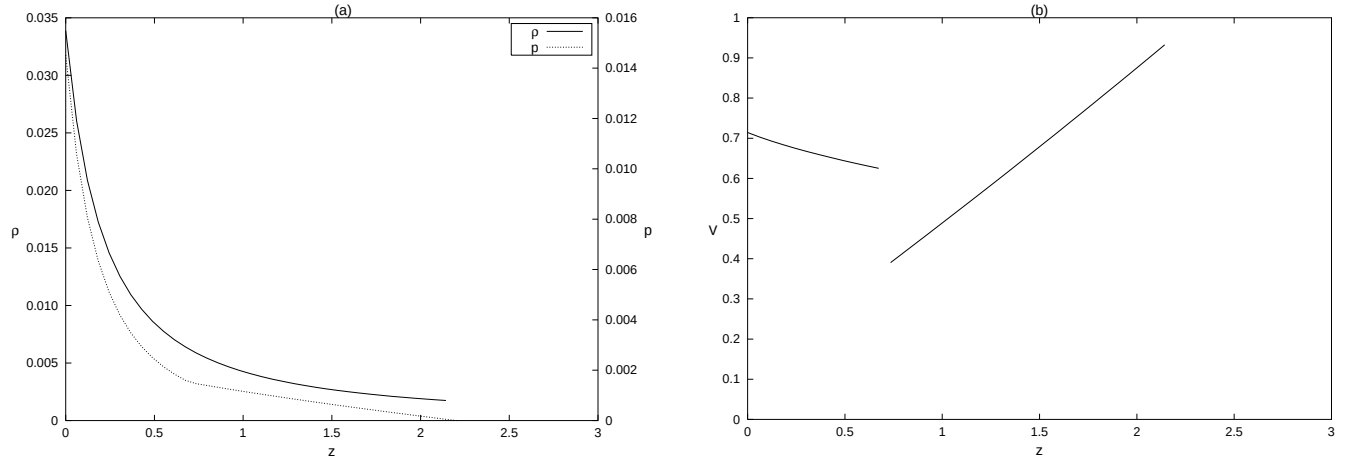

FIG. 24. (a) The density ρ and pressure p, and (b) the velocity of sound, V for the halo formed by fluid layers, Eqs. (81) and (82), with $r_1=1$ and $r_2=2$ for $a=0.3$ along the z axis.

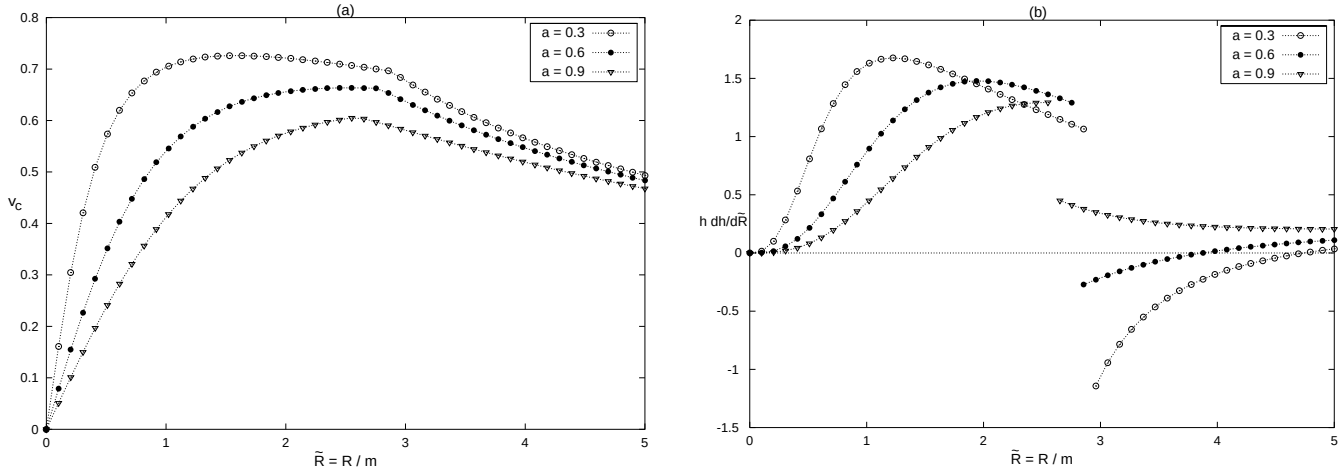

FIG. 25. (a) The tangential velocity v_c and (b) the curves of $hdh/d\tilde{R}$ for the disk generated from spherical fluid layers, Eqs. (81) and (82), with $r_1=1$ and $r_2=2$, for $a=0.3$, 0.6, and 0.9 as functions of $\tilde{R}=R/m$. Regions of unstable circular orbits appear for the disks obtained with parameters $a=0.3$ and 0.6.

$$A_1=0, A_2=\frac{1}{\sqrt{C}},$$

$$B_2=\frac{r_1^{\sqrt{2}}}{2\sqrt{2C}}\{[A_3+B_3\ln(r_1)](1-r_1^{-\sqrt{2}})+2\sqrt{2}B_3\}, \tag{85}$$

$$B_1=\frac{r_1^{\sqrt{2}}}{2\sqrt{2C}}\{[A_3+B_3\ln(r_1)][2\sqrt{2}r_1^{-\sqrt{2}}-\ln(r_1)+\ln(r_1)r_1^{-\sqrt{2}}]-2\sqrt{2}B_3\ln(r_1)\}. \tag{86}$$

Using Eqs. (43) and (66), the energy density of the disk at $R=\sqrt{r_1^2-a^2}$ is continuous, but not the pressure. The difference between Eqs. (68) and (45) is

$$\Delta P=\frac{a(r_1^{\sqrt{2}/2}-r_1^{-\sqrt{2}/2})}{16\pi\sqrt{C}r_1[A_3+B_3\ln(r_1)]}\{\sqrt{2}[A_3+B_3\ln(r_1)]+4B_3\}. \tag{87}$$

The pressure is continuous if $r_1^{\sqrt{2}/2}-r_1^{-\sqrt{2}/2}=0\rightarrow r_1=1$.

Figures 23(a)–23(c) show, respectively, σ, P, and V for the disk obtained from fluid layers (81) and (82) with parameters $r_1=1$ and $r_2=2$ for $a=0.3$,0.6, and 0.9 as functions of $\tilde{R}=R/m$. The density ρ, pressure p, and velocity of sound, V, for the halo along the z axis with the same parameters for $a=0.3$ are shown in Figs. 24. In Figs. 25(a) and 25(b), the curves of tangential velocities and of $hdh/d\tilde{R}$, respectively, are displayed as functions of $\tilde{R}=R/m$. In this case, regions of unstable orbits exist for parameters $a=0.3$ and $a=0.6$.

VI. DISCUSSION

The displace, cut, and reflect method applied to solutions of Einsteins field equations in isotropic coordinates can generate disks with positive energy density and equal radial and azimuthal pressures (perfect fluid). With solutions of static spheres of a perfect fluid it is possible to construct disks of the perfect fluid surrounded also by a perfect fluid matter. As far we know these are the first disk models of this kind in the literature.

TABLE I. Disks properties.

Solution	Metric coefficients	Matching conditions	Energy density	Pressure	Sound velocity	Angular momentum
External Schwarzschild	(9)		(10)	(11)	(13)	(23)
Buchdahl	(24)		(27)	(28)	(29)	(31)
NPV 1a	(32), (33)	(40), (41)	(43)	(44)	(46)	(50)
NPV 1b	(32), (34)	(40), (42)	(43)	(45)	(47)	(51)
NPV 2a	(52), (53)	(60)–(63)	(66)	(67)	(69)	(73)
NPV 2b	(52), (54)	(60), (61), (64), (65)	(66)	(68)	(70)	(74)
Internal Schwarzschild +Buchdahl	(75), (76)	(77)–(80)	(66), (27)	(67), (28)	(69), (29)	(73), (31)
NPV 2b+NPV 1b +external Schwarzschild	(81), (82), (83)	(84)–(86)	(66), (43), (10)	(68), (45), (11)	(70), (47), (13)	(74), (51), (23)

All disks constructed as examples have some common features: surface energy density and pressures decrease monotonically and rapidly with radius. As the ''cut'' parameter a decreases, the disks become more relativistic, with surface energy density and pressure more concentrated near the center. Also regions of unstable circular orbits are more likely to appear for highly relativistic disks. Parameters can be chosen so that the sound velocity in the fluid and the tangential velocity of test particles in circular motion are less than the velocity of light. This tangential velocity first increases with radius and reaches a maximum. Then, for large radii, it decreases as $1/\sqrt{R}$, in case of disks generated from Schwarzschild and Buchdahl's solutions. The sound velocity is also a decreasing function of radius, except in solution NPV 2a with $\sqrt{2}<n\leqslant 2$, where it reaches its maximum value at the boundary. In principle, other solutions of static spheres of perfect fluid could be used to generate other disk + halo configurations, but it is not guaranteed that the disks will have the characteristics of normal fluid matter.

We believe that the presented disks can be used to describe a more realistic model of galaxies than most of the already studied disks since the counterrotation hypothesis is not needed to have a stable configuration.

We want to finish our discussion by presenting a table that summarizes our results about disks in a unified manner.

In Table I we list the seed metric coefficients, matching conditions at the boundaries, and relevant physical quantities of all disks studied in this work. The numbers refer to the equations presented along the paper and NPV stands for Narlikar, Patwardhan, and Vaidya as before.

ACKNOWLEDGMENTS

We want to thank FAPESP, CAPES, and CNPQ for financial support.

[1] W.A. Bonnor and A. Sackfield, Commun. Math. Phys. **8**, 338 (1968).
[2] T. Morgan and L. Morgan, Phys. Rev. **183**, 1097 (1969).
[3] L. Morgan and T. Morgan, Phys. Rev. D **2**, 2756 (1970).
[4] G. González and P.S. Letelier, Class. Quantum Grav. **16**, 479 (1999).
[5] T. Ledvinka, M. Zofka, and J. Bičák, in *Proceedings of the 8th Marcel Grossman Meeting in General Relativity*, edited by T. Piran (World Scientific, Singapore, 1999), pp. 339–341.
[6] P.S. Letelier, Phys. Rev. D **60**, 104042 (1999).
[7] J. Katz, J. Bičák, and D. Lynden-Bell, Class. Quantum Grav. **16**, 4023 (1999).
[8] D. Lynden-Bell and S. Pineault, Mon. Not. R. Astron. Soc. **185**, 679 (1978).
[9] J.P.S. Lemos, Class. Quantum Grav. **6**, 1219 (1989).
[10] J.P.S. Lemos and P.S. Letelier, Class. Quantum Grav. **10**, L75 (1993).
[11] J.P.S. Lemos and P.S. Letelier, Phys. Rev. D **49**, 5135 (1994).
[12] J.P.S. Lemos and P.S. Letelier, Int. J. Mod. Phys. D **5**, 53 (1996).
[13] C. Klein, Class. Quantum Grav. **14**, 2267 (1997).
[14] J. Bičák, D. Lynden-Bell, and J. Katz, Phys. Rev. D **47**, 4334 (1993).
[15] J. Bičák, D. Lynden-Bell, and C. Pichon, Mon. Not. R. Astron. Soc. **265**, 126 (1993).
[16] O. Semerák, in *Gravitation: Following the Prague Inspiration*, to Celebrate the 60th Birthday of Jiri Bičák, edited by O. Semerák, J. Podolsky, and M. Zofka (World Scientific, Singapore, 2002), p. 111, available at http://xxx.lanl.gov/abs/gr-qc/0204025.
[17] G.G. Kuzmin, Astron. Zh. **33**, 27 (1956).
[18] A.H. Taub, J. Math. Phys. **21**, 1423 (1980).
[19] J.P.S. Lemos and P.S. Letelier, Phys. Lett. A **153**, 288 (1991).
[20] Lord Rayleigh, Proc. R. Soc. London **A93**, 148 (1916).
[21] L. D. Landau and E. M. Lifshitz, *Fluid Mechanics*, 2nd ed. (Pergamon, Oxford, 1987), Sec. 27.
[22] B. Kuchowicz, Acta Phys. Pol. B **3**, 209 (1972).
[23] H.A. Buchdahl, Astrophys. J. **140**, 1512 (1964).
[24] V.V. Narlikar, G.K. Patwardhan, and P.C. Vaidya, Proc. Natl. Inst. Sci. India, **9**, 229 (1943).